Atmos. Chem. Phys., 25, 11157–11182, 2025
https://doi.org/10.5194/acp-25-11157-2025

Atmospheric Chemistry and Physics
Open Access
EGU

Research article

Adiabatic and radiative cooling are both important causes of aerosol activation in simulated fog events in Europe

Pratapaditya Ghosh[1,2], Ian Boutle[3], Paul Field[3,4], Adrian Hill[3,5], Marie Mazoyer[6], Katherine J. Evans[7], Salil Mahajan[7], Hyun-Gyu Kang[7], Min Xu[7], Wei Zhang[7], and Hamish Gordon[8,2]

[1]Department of Civil and Environmental Engineering, Carnegie Mellon University, 5000 Forbes Avenue, Pittsburgh, PA 15213, USA
[2]Center for Atmospheric Particle Studies, Carnegie Mellon University, 5000 Forbes Avenue, Pittsburgh, PA 15213, USA
[3]Met Office, Fitzroy Road, Exeter, EX1 3PB, UK
[4]School of Earth and Environment, University of Leeds, Leeds, LS2 9JT, UK
[5]European Centre for Medium-Range Weather Forecasts, Reading, UK
[6]CNRM, Université de Toulouse, Météo-France, CNRS, Toulouse, France
[7]Oak Ridge National Laboratory, Oak Ridge, TN 37831, USA
[8]Department of Chemical Engineering, Carnegie Mellon University, 5000 Forbes Avenue, Pittsburgh, PA 15213, USA

Correspondence: Hamish Gordon (gordon@cmu.edu)

Received: 31 October 2024 – Discussion started: 16 December 2024
Revised: 16 June 2025 – Accepted: 18 June 2025 – Published: 24 September 2025

Abstract. Aerosol–fog interactions affect the visibility in, and life cycle of, fog and are difficult to represent in weather and climate models. Here we explore processes that impact the simulation of fog droplet number concentrations (N_d) at sub-kilometer scale horizontal grid resolutions in the UK Met Office Unified Model. We modify the parameterization of aerosol activation to include droplet activation by radiative cooling in addition to adiabatic cooling and determine the relative importance of the two cooling mechanisms. We further test the sensitivity of simulated N_d to: (a) interception of droplets by trees and buildings, (b) overestimation of updrafts in temperature inversions (which leads to artificially high N_d values), and (c) potential mechanisms for droplet deactivation due to downward fluctuations in supersaturation.

We evaluate our model against observations from the ParisFog and LANFEX field campaigns, building on evaluation described in the companion paper. Including radiative cooling in the activation mechanism improves how accurately we represent the liquid water path and the vertical structure of the fog in our LANFEX case study. However, with radiative cooling, the N_d are overestimated for most of the ParisFog cases and for the LANFEX case. The time-averaged overestimate exceeds a factor of three (the normalized mean bias factor exceeds 2.0) in 4 out of 11 ParisFog cases. Our sensitivity studies demonstrate how these overestimates can be mitigated. Assuming the overestimate affects both radiative and adiabatic cooling, we find that although radiative cooling is more often the dominant source, both cooling sources can sometimes dominate activation.

Published by Copernicus Publications on behalf of the European Geosciences Union.

1 Introduction

Aerosol–cloud and aerosol–fog interactions are complex and often represented in a simplified way in weather and climate models (Boutle et al., 2018; Mazoyer et al., 2019, 2022; Poku et al., 2019, 2021). The effects of aerosols on the optical properties and life cycle of fog, and resulting effects on Earth's radiative balance, are uncertain (Twomey, 1977; Albrecht, 1989). Low visibility due to fog leads to hazardous conditions, especially for transportation, and results in financial losses (Leung et al., 2020; Kulkarni et al., 2019; Peng et al., 2018; Hao et al., 2017; Abdel-Aty et al., 2011; Gultepe et al., 2007). Lakra and Avishek (2022) provides a broad description of the scientific and social importance of fog. Forecasting the fog life cycle accurately in numerical weather prediction models is challenging (Boutle et al., 2018; Pithani et al., 2019; Jayakumar et al., 2021; Smith et al., 2021; Kutty et al., 2021; Mazoyer et al., 2022). In the cloud microphysics components of most weather prediction and climate models, aerosols, whether represented prognostically or using climatologies, are usually activated to cloud and fog droplets assuming that adiabatic cooling is the only source of supersaturation. Some models have separate parameterizations to predict visibility (e.g., Clark et al., 2008); however, in cases we are aware of, the visibility parameterization does not inform other parts of the model – for example, the cloud microphysics and radiative transfer schemes.

Radiation fog is characterized by radiative cooling at night, clear skies, and calm conditions. The start of the fog is driven by radiative cooling and with time the fog layer gradually transitions to a well-mixed fog layer in which adiabatic cooling is also active (Maronga et al., 2015; Boutle et al., 2018). In large eddy simulation studies, and probably in reality, droplets can be activated via both radiative and adiabatic cooling (Poku et al., 2021).

In the companion paper (Ghosh et al., 2025c), we evaluated the ability of the UK Met Office Unified Model with interactive double-moment aerosol and cloud microphysics to simulate fog at 500 m grid resolution in case studies from the ParisFog field campaign in 2011. We demonstrated strategies to improve fog droplet number concentrations (N_d) while activating the droplets via adiabatic cooling only. While the default model significantly underestimated droplet concentrations, we found that either including an updated version of the aerosol activation parameterization by Abdul-Razzak and Ghan (2000) following Ghosh et al. (2025a), or including a contribution to updraft speeds from sub-grid scale turbulence, could substantially improve model performance. Here, in this paper, we explore the contribution of radiative cooling to activation in the same fog cases and we additionally examine a single case study from the Local and Non-Local Fog Experiment (LANFEX) field campaign in 2014 (Price et al., 2018; Price, 2019), for which we have vertical profiles of fog droplet concentrations.

Several existing simulation studies with bulk aerosol and cloud microphysics schemes include radiative cooling in their activation code. Following Stolaki et al. (2015), Mazoyer et al. (2017) simulated a fog event during the ParisFog field campaign (Haeffelin et al., 2010) using the Meso-NH (Lac et al., 2018) large-eddy simulation (LES) model and found that radiative cooling was the main source of droplet activation. Poku et al. (2021) simulated a fog event during the LANFEX campaign using the Met Office Natural Environment Research Council (NERC) Cloud (MONC) LES model (Brown et al., 2015, 2018) and demonstrated very high contributions of radiative cooling to aerosol activation, sometimes up to 100 %. Duconge et al. (2020) and Vié et al. (2024) also simulated the fog vertical structure during LANFEX using the Meso-NH model with radiative cooling included. However, LES simulations cannot readily be used to predict the weather or future climate and are often run in idealized frameworks that only rarely include fully prognostic interactive aerosol and realistic space- and time-varying large-scale forcing via non-periodic boundary conditions. Although there are studies that use numerical weather prediction (NWP) models, such as Jia et al. (2019), Jayakumar et al. (2021), Yan et al. (2021), and Parde et al. (2022), most of these studies use either a single-moment cloud microphysics scheme in which droplet number concentrations are not prognostic, or they do not include aerosol activation by radiative cooling. An exception is a recent NWP study of fog with aerosol-aware microphysics in the WRF model by Peterka et al. (2024), who found an increase in droplet concentration of around a factor of three resulted from including activation by radiative cooling. In view of the significant changes found when radiative cooling is included in these simulations, therefore, it is useful to continue to explore including activation by radiative cooling in cloud microphysics schemes used in weather and climate models.

The simple and computationally inexpensive "ARG" aerosol activation parameterization developed by Abdul-Razzak and Ghan (2000) is very popular in different research models used for both weather and climate, including the WRF-Chem model (Grell et al., 2005; Fast et al., 2006), the Community Earth System Model (CESM, Danabasoglu et al., 2020), Energy Exascale Earth System Model (E3SM, Golaz et al., 2022), and the UK Met Office Unified Model in both high-resolution (Field et al., 2023; Gordon et al., 2023) and climate configurations such as the UK Earth System Model (UKESM, Mulcahy et al., 2023). The ARG scheme was designed for low-level warm clouds, but we showed in the companion paper that it can perform well in fog, though it should ideally be modified in polluted conditions where kinetic limitations on droplet activation are important. It can also be modified straightforwardly (Peterka et al., 2024) to include radiative cooling, similar to the Shipway and Hill (2012) activation scheme (Poku et al., 2021). However, it is unclear whether including activation by radiative cooling will improve or worsen the scheme's performance in a numeri-

cal weather prediction setup that must simulate all types of cloud, including but not limited to fog.

In situations like fog, the resolved updraft speeds are very low. To preserve numerical stability and act as a proxy for non-adiabatic sources of cooling in such cases, most models use a minimum updraft speed, or a minimum width of a distribution of updraft speeds, to activate aerosols in the ARG parameterization (Sullivan et al., 2016; Boutle et al., 2018). A minimum updraft speed of $0.01\,\mathrm{m\,s^{-1}}$ is equivalent to a cooling rate of $0.23\,\mathrm{K\,h^{-1}}$ assuming a $6.5\,\mathrm{K\,km^{-1}}$ temperature lapse rate. In such simulations, droplet concentrations are determined not by the actual cooling rate but by the minimum updraft speed, which is not a global constant but varies with time and space as the fog evolves. Only by including radiative cooling explicitly can this spatial and temporal dependence of non-adiabatic activation be represented in models.

Activation is not the only parameterized process in our model and biases in different parameterizations can lead to compensating errors. We explore the possible effect of other processes on the droplet concentration to some extent here in sensitivity studies, aiming to maintain reasonable good agreement with observations. The interception of fog droplets by trees and buildings could be an important droplet sink (Mazoyer et al., 2017), which is not included by default in NWP models since cloud microphysics schemes are not designed for fog in general. The entrainment of warm air could result in additional mixing and evaporation of droplets through entrainment–evaporation feedback (Ackerman et al., 2004; Bretherton et al., 2007; Barahona and Nenes, 2007). Fog droplets can undergo collision coalescence or Ostwald ripening (Degefie et al., 2014; Mazoyer et al., 2019, 2022) and form larger and fewer droplets. In specific foggy conditions, Boutle et al. (2018) also found a similar configuration of the model we used overestimated updraft speeds. We explore the influence of these effects on simulated N_d.

In this study, we simulate the fog life cycle during the ParisFog (Haeffelin et al., 2010) field campaign in 2011, following the companion paper (Ghosh et al., 2025c). In addition, we simulate a fog event during the LANFEX field campaign in 2014 to study the vertical profile of fog droplets (N_d) and the liquid water path. In Sect. 2, we provide an overview of the measurements and the model setup we use in this study. We then proceed to introduce radiative cooling as a mechanism for aerosol activation and explore various sensitivity analyses. Compared to the companion paper, these sensitivity studies generally represent explorations of possible developments to the model physics and are not simply updating parameters. Following this, we evaluate the model's performance in detail. Finally, we discuss the relative importance of adiabatic and radiative cooling processes and conclude the paper.

2 Measurements and model description

We use the same set of aerosol and cloud measurements from the 11 radiation and stratus lowering fog events from 15–25 November 2011 during the ParisFog field campaign we describe in the companion paper. In brief, we evaluated our simulations using observations from the Scanning Mobility Particle Sizer (SMPS), the Palas Welas-2020 Particle Counter (WELAS), and the DMT Fog Monitor (FM-100) located at the SIRTA observatory near Paris. We also used surface temperature measurements, radiosonde data, and satellite observations.

In addition, for this paper we use observations from the Intensive Observation Period (IOP) 1 of LANFEX (Price et al., 2018) during the night of 24–25 November 2014 at the Met Office observation site in Cardington, Bedfordshire, UK. The LANFEX campaign, an extension from the Cold-Air Pooling Experiment (COLPEX; Price et al., 2011), was designed to study the life cycle of radiation fog in Bedfordshire and Shropshire in England, using field measurements and numerical simulations. This campaign also aimed at understanding the vertical growth of fog layers and the relative importance of local and non-local processes on radiation fog. The 24–25 November nocturnal fog case has been extensively studied, first in a dedicated LES model (Boutle et al., 2018), and then in a model intercomparison study which compared and evaluated LES and single column models (Boutle et al., 2022). Two LES studies have previously used this IOP to study aerosol activation specifically (Poku et al., 2021; Vié et al., 2024). While the intercomparison highlighted progress in modeling the fog onset compared to earlier model intercomparison studies (Bergot et al., 2007), models still deviated substantially from observations of fog properties, reflecting the difficulty of forecasting fog. To evaluate our simulations of the IOP, we use observations including temperature and relative humidity (RH) profiles from radiosondes, vertical profiles of N_d and liquid water content (LWC) from a cloud droplet probe on a tethered balloon, and liquid water path measurements from a radiometer.

We use the same model configuration as described in the companion paper. In summary, we use the UK Met Office Unified Model (UM), where a global model (with a horizontal resolution of $1.87° \times 1.25°$) drives two nested regional domains of resolution 4 km and 500 m centered on the SIRTA observatory (48.713° N, 2.208° E) in Paris (for ParisFog 2011) and the Met Office observational site (52.1015° N, 0.4159° W) at Cardington, UK (for LANFEX 2014). Each regional model domain has 300×300 grid boxes horizontally and 70 vertical levels extending to 40 km altitude. We use the RA3 model configuration (Bush et al., 2025) with the bimodal cloud parameterization replaced by the Smith et al. (1990) parameterization, as in the companion paper, to ensure sufficient coverage of fog. Our simulations use the double-moment aerosol microphysics scheme Global Model of Aerosol Processes (GLOMAP, described

by Mann et al., 2010, 2012) coupled to the double-moment cloud microphysics scheme Cloud AeroSol Interacting Microphysics (CASIM, described by Shipway and Hill, 2012; Grosvenor et al., 2017; Gordon et al., 2020; Field et al., 2023) to study fog at high spatial resolution. Our simulations include nitrate aerosols (Jones et al., 2021) in addition to other aerosol species, such as black carbon, organic carbon, and sulfate. We use the StratTrop chemistry scheme within the UK Chemistry and Aerosol (UKCA) submodel (Archibald et al., 2020; Gordon et al., 2023) in this study. This relatively complex chemistry mechanism, which predicts ozone prognostically, is required by the nitrate scheme. As discussed in more detail in Sect. 3, all simulations use the ARG activation scheme to activate aerosols, using updraft speeds diagnosed at the grid scale with no additional contribution from sub-grid-scale turbulence but with a minimum updraft speed of $0.01\,\mathrm{m\,s^{-1}}$.

All results presented in this paper are from our 500 m horizontal resolution model domains for ParisFog and LANFEX. The domain locations are shown on the left panels of Fig. 1. The middle panels show the urban surface tiles in the 500 m resolution model, with the measurement sites at the SIRTA observatory and at Cardington as black circles. The right panel shows surface elevation (m); the Seine and Thames river basins are visible in the center and extreme south of the domains, respectively.

3 Aerosol activation experiments

In the companion paper, we showed that our model setup for ParisFog with the standard ARG activation scheme significantly underpredicts droplet numbers. The underprediction is likely due to a combination of deficiencies in the ARG activation parameterization and the underestimation of updrafts that results from not including sub-grid turbulence. When we implemented an updated version of the ARG scheme, following the approach of Ghosh et al. (2025a), we were able to predict droplet concentrations reasonably accurately. We additionally updated the aerosol hygroscopicities, though this made relatively little difference to these simulations. Our updated configuration, labeled "AD" for "adiabatic cooling" below, serves as the baseline simulation in this study. For context, we also show some results here from simulations with the standard ARG activation scheme, labeled Def-ARG. In the companion paper, we demonstrated that accounting for sub-grid turbulence in addition to our updates to the ARG parameterization would lead to overestimation of N_d. Given this bias and the uncertainties around how best to parameterize the contribution of sub-grid turbulence to activation, we do not use a sub-grid turbulence component in any of the new simulations we present here. These simulations are described in the following subsections.

3.1 Radiative + diabatic cooling (AD-RAD)

Fog usually forms in stable boundary layers. Depending on the balance between mechanical and thermal turbulence, the stable boundary layer can vary from well-mixed to non-turbulent (Stull, 1988). The heat budget inside such a layer is as follows:

$$Q_\mathrm{total} = Q_\mathrm{W} + Q_\mathrm{R} + Q_\mathrm{E} + Q_\mathrm{SH} + Q_\mathrm{LH} + Q_\mathrm{S}. \quad (1)$$

The total heat flux Q_total has several components: fluxes from adiabatic cooling Q_W that depend on updrafts, longwave radiative cooling Q_R, mixing by entrainment Q_E, sensible heat Q_SH, latent heat Q_LH, and subsidence heating Q_S. Updrafts are expected to be low in a stable boundary layer, but sometimes dominate the cooling rate, for example in an "adiabatic fog" (Boutle et al., 2018). At night, the ground surface cools as it emits infra-red radiation. The cooling rates typically vary between 0.5 and $3\,\mathrm{K\,h^{-1}}$. We assume that adiabatic and radiative cooling are the most important sources of supersaturation in radiation fog. In Meso-NH LES simulations, Vié et al. (2024) additionally include surface sensible and latent heat fluxes and turbulent fluxes of temperature while Mazoyer et al. (2017) do not; these terms were not clearly shown to be important, but could be explored in future studies.

In our first sensitivity simulation (termed AD-RAD hereafter), we introduce radiative cooling in the ARG activation scheme following the work of Poku et al. (2021) and Peterka et al. (2024), in addition to changes in simulation "Mod-Kappa" described in the companion paper (termed "AD" in this part) of the study (i.e., updated ARG scheme and with modified hygroscopicities). In the def-ARG and AD simulations, the change in supersaturation $\frac{\mathrm{d}s}{\mathrm{d}t}$ is represented as:

$$\frac{\mathrm{d}s}{\mathrm{d}t} = \psi_1 \frac{\mathrm{d}T}{\mathrm{d}t}\bigg|_\mathrm{ad} - \gamma \frac{\mathrm{d}q}{\mathrm{d}t}. \quad (2)$$

In Eq. (2), the term $\frac{\mathrm{d}T}{\mathrm{d}t}\big|_\mathrm{ad}$ represents the adiabatic cooling rate, which is given by $-\Gamma w$. Here, $\Gamma = \frac{g}{c_\mathrm{p}}$ denotes the adiabatic lapse rate, where g is the gravitational acceleration, c_p is the specific heat capacity of air, and w refers to the updraft velocity. The prefactor ψ_1 is defined as $\psi_1 = \frac{c_\mathrm{p}}{R_\mathrm{a}T} - \frac{L}{R_\mathrm{v}T^2}$, where R_a and R_v are the gas constants for dry air and water vapor, respectively, L is the latent heat of vaporization, and T is the ambient air temperature. This term is the source of supersaturation from adiabatic cooling generated by the updrafts.

The second term is the sink of supersaturation (condensation of water onto aerosol particles and pre-existing droplets), which is dependent on the rate of latent heat release due to condensation of water, $\frac{\mathrm{d}q}{\mathrm{d}t}$. The prefactor γ can be written as: $\gamma = \frac{p}{\epsilon e_\mathrm{s}} + \frac{L_2}{R_\mathrm{v}T_2 c_\mathrm{p}}$. Here, p is the pressure of dry air and $\epsilon = \frac{R_\mathrm{a}}{R_\mathrm{v}} = 0.622$.

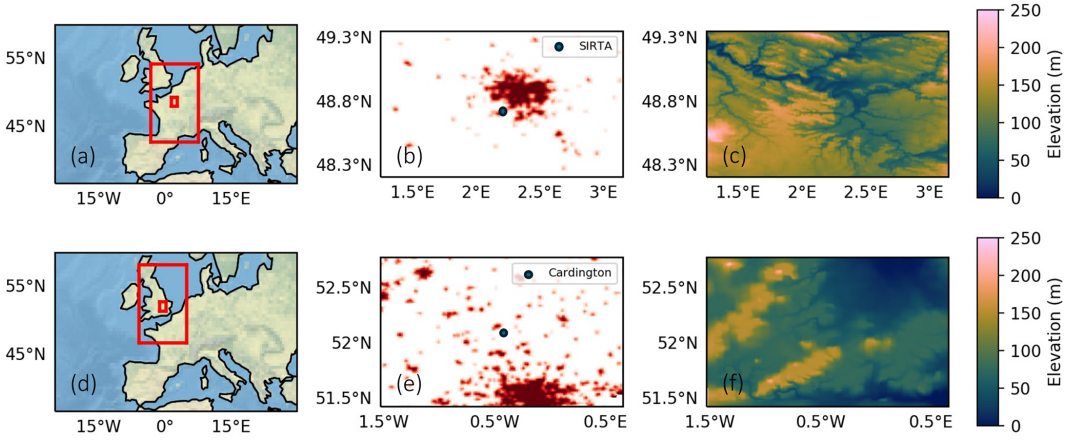

Figure 1. Panels **(a)** and **(d)** show the two nested domains of grid spacing 4 km (outer domain) and 500 m (inner domain) used in this study for ParisFog **(a)** and LANFEX **(d)**. Both domains have 300 grid points in the latitude and longitude directions. Panels **(b)** and **(e)** show urban grid cells in the 500 m resolution model domains for ParisFog **(b)** and LANFEX **(e)**. Panels **(c)** and **(f)** show surface altitude (m) in the same two 500 m resolution domains.

To introduce radiative cooling, we add an additional source term $\psi_2 \frac{\mathrm{d}T}{\mathrm{d}t}\Big|_{\mathrm{rad}}$ in the above equation, which now becomes:

$$\frac{\mathrm{d}s}{\mathrm{d}t} = \psi_1 \frac{\mathrm{d}T}{\mathrm{d}t}\Big|_{\mathrm{ad}} + \psi_2 \frac{\mathrm{d}T}{\mathrm{d}t}\Big|_{\mathrm{rad}} - \gamma \frac{\mathrm{d}q}{\mathrm{d}t}. \tag{3}$$

In Eq. (3), the radiative cooling rate is represented by $\frac{\mathrm{d}T}{\mathrm{d}t}\Big|_{\mathrm{rad}}$ and the prefactor ψ_2 is defined as: $\psi_2 = -\frac{L}{R_v T^2}$. We considered both the longwave cooling and shortwave heating predicted by the UM's radiation scheme to calculate the net radiative cooling rate and included it in the activation scheme.

As demonstrated in the "Results" section, including radiative cooling tends to lead to our simulations overpredicting droplet number concentrations. We explore possible reasons for an overprediction in the remaining sensitivity studies.

3.2 Fog deposition (AD-RAD-SED)

Interception by plant canopies, buildings, and other structures is an important sink of fog droplets (Mazoyer et al., 2017) as they move in turbulent flow near the surface. Sedimentation of cloud droplets is represented in our model, so droplets are lost if they settle out from the lowest model level, but there is no additional parameterization of droplet interception or inertial impaction close to the surface. The LES study of fog by Mazoyer et al. (2017) introduces an additional fog deposition term in the lowest level of their model to account for interception. Taylor et al. (2021) also introduced a similar parameterization for losses due to interception in the WRF model to better simulate LWC and visibility in marine fog.

For our model, the sedimentation (gravitational settling) velocity of a droplet of diameter D, V_{sed}, is (Field et al., 2023):

$$V_{\mathrm{sed}} = a D^b \left(\frac{\rho_0}{\rho}\right)^f. \tag{4}$$

In this equation, $a = 3.0 \times 10^7\ \mathrm{m^{-1}\,s^{-1}}$, $b = 2.0$, $\rho_0 = 1.2\ \mathrm{kg\,m^{-3}}$ (reference air density), and $f = 0.50$. From this equation, $V_{\mathrm{sed}} = 0.30\ \mathrm{cm\,s^{-1}}$ for a 10 µm diameter droplet and $V_{\mathrm{sed}} = 0.675\ \mathrm{cm\,s^{-1}}$ for a 15 µm droplet.

To account for interception as well as sedimentation, Mazoyer et al. (2017) used a fixed $2\ \mathrm{cm\,s^{-1}}$ fog droplet deposition velocity (V_{dep}), while Katata (2014) suggested a 2.1–8 $\mathrm{cm\,s^{-1}}$ range of V_{dep} for short vegetation. Nelli et al. (2024) estimated fog deposition velocities to be in the range of 0.13–3.26 $\mathrm{cm\,s^{-1}}$ (mean = $1.70\ \mathrm{cm\,s^{-1}}$) for LWC 0–0.1 $\mathrm{g\,m^{-3}}$ (typical for our fog cases). Therefore, in this simulation (hereafter termed AD-RAD-SED), in addition to previous changes, we scale up the sedimentation flux (for both the mass and number of cloud droplets) by a factor of 3 in the lowest model level as a proxy for the interception of droplets. From Eq. (4), the effective deposition velocity is then $0.9\ \mathrm{cm\,s^{-1}}$ for a 10 µm droplet and $2.02\ \mathrm{cm\,s^{-1}}$ for a 15 µm droplet, comparable to these other studies. Although realistic, this crude scaling factor would need refining before being included in a default model configuration.

3.3 No activation in inversion (AD-RAD-INV)

In Fig. S1 (right panel) in the Supplement, from the 500 m model, we show the standard deviation (σ_{w}) of the unresolved vertical velocity in the foggy grid boxes for two ParisFog cases and the LANFEX case in the lowest model level (5 m altitude). We find that for the AD-RAD simulation, σ_{w} is about a factor of 5 higher than LANFEX observations.

Radiosonde profiles shown later in Sect. 4.1, and simulated temperature gradients shown in Fig. S2, show that the

fog observed during LANFEX IOP1 occurred in a strong temperature inversion. In a temperature inversion, updraft speeds are expected to be close to zero and often negative (see Fig. 4 of Stolaki et al., 2015) because the rising air parcels immediately become cooler than the surrounding air, so they lose their buoyancy. In the model, on average, the resolved updraft in the foggy grid boxes is close to zero, but there are multiple grid boxes where updrafts are positive.

As discussed in the companion paper, in the model, a minimum updraft threshold of $0.01\,\mathrm{m\,s^{-1}}$ is applied in the activation parameterization and there is no contribution to updrafts from sub-grid-scale turbulence. As we discuss in the next subsection, the activation scheme updates N_d on each time step if it exceeds the N_d already present in the grid box, and so the N_d depends on the highest updraft speed since the formation of the fog, likely similar to the maximum shown in the left and middle panels of Fig. S1. For the LANFEX case study, fewer than 10 % of the resolved updrafts exceed the threshold throughout the fog layer, but for ParisFog, updrafts can be greater than $0.01\,\mathrm{m\,s^{-1}}$ for 20 %–30 % of the grid boxes that have positive updrafts while the temperature is increasing with height, as shown in Fig. S2. Even though these resolved updraft speeds are usually small, below $0.02\,\mathrm{m\,s^{-1}}$ at the surface, they do seem to result in significant activation and it is not clear whether such high resolved updraft speeds within the inversion are physical or are an artifact of the model's boundary layer scheme.

We hypothesize that activation by adiabatic cooling inside strong temperature inversions should be unlikely, due to weak updrafts and potentially also mixing with subsiding warmer air. In our next sensitivity study, we implement a switch in the activation scheme that suppresses updraft-driven activation when the temperature profile gradient is positive (indicating an inversion). Our simulation, hereafter denoted AD-RAD-INV, incorporates the changes from simulation AD-RAD and this suppression of activation in temperature inversions, which means that aerosols can only activate via radiative cooling when temperature increases with height. Figure 2 shows the resulting decision tree for droplet activation in the AD-RAD-INV simulation.

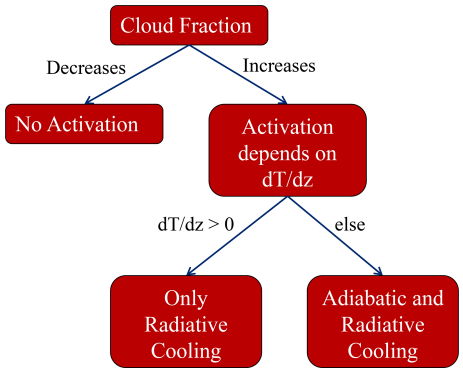

Figure 2. This figure shows a flowchart of droplet activation in simulation AD-RAD-INV. The "ARG" activation scheme is called when cloud fraction increases. Activation is suppressed in temperature inversions. The workflow for simulation AD-RAD is similar, except that activation proceeds independently of $\mathrm{d}T/\mathrm{d}z$ (the rate of change in temperature with height).

3.4 Droplet concentration adjustment timescale (AD-RAD-DCAT)

In the CASIM cloud microphysics scheme, Eq. (5) shows how the droplet number concentration in the model changes from one time step to the next. The droplet concentration from the previous time step ("Old N_d") is altered by advection and microphysical processes other than activation, such as sedimentation, accretion, or riming, before the activation scheme is called. We call N_d after advection and microphysics but before activation the "pre-activation N_d" and the updated droplet concentration of the current time step "New N_d".

$$\begin{aligned}\text{New } N_\mathrm{d} = \text{Old } N_\mathrm{d} + \Delta N_{\mathrm{d,Advection}} + \Delta N_{\mathrm{d,Microphysics}} \\ + \Delta N_{\mathrm{d,Activation}} = \text{Pre-activation } N_\mathrm{d} \\ + \Delta N_{\mathrm{d,Activation}} \end{aligned} \quad (5)$$

Furthermore, there is the additional constraint that $\Delta N_{\mathrm{d,Activation}}$ can only be positive; if fewer droplets are activated than currently exist, $\Delta N_{\mathrm{d,Activation}}$ is set to zero. If the cloud fraction calculated in the model decreases, the droplets evaporate proportionally to the decrease in the cloud fraction. However, during the entire life cycle of fog, if the fog cover in a grid box (as calculated by the Smith (1990) parameterization) remains the same or increases, there is no mechanism to reduce the droplet concentration in that grid box except sedimentation (and interception, as included in our study), losses to ice or precipitation, and advection.

In reality, several other processes may reduce the droplet concentration (or the concentration of droplet-sized particles) during a fog once droplets are formed, but these processes are not included in our model. These include the deactivation of droplets in downward fluctuations in relative humidity (Prabhakaran et al., 2020), collision-coalescence (e.g., Xue et al., 2008; Zhao et al., 2013), Ostwald ripening (e.g., Yang et al., 2018; Mazoyer et al., 2022), or the shrinkage of large, hydrated, but unactivated aerosols that were previously large enough to be detected by a fog monitor or cloud droplet probe. In our model, there are insignificant numbers of unactivated aerosols with an ambient (wet) diameter greater than 2 µm (see Fig. S4 of the companion paper), yet Mazoyer et al. (2019) find ambient activation diameters in excess of 3 µm (using measurements and κ–Köhler theory) and significant corresponding "droplet" concentrations.

We introduce the concept of "droplet concentration adjustment timescale (DCAT)" as a proxy for all these other pro-

cesses that can lead to N_d decreasing over time. We assume that the memory of the maximum supersaturation at which the droplets were activated persists only for a certain time; if the supersaturation decreases, the droplet concentration slowly adjusts to correspond to the concentration that would activate at the subsequent, lower, supersaturations. From the standard equations for droplet growth (e.g., Seinfeld and Pandis, 1998), we calculate that it would take around 700 s for a 15 µm droplet to evaporate to a 1 µm aerosol when the supersaturation changes by 0.05 % (relative humidity changes from 100.0 % to 99.95 %), at 283 K. Small supersaturation changes are likely in fog. Thus, we impose a linearly decaying memory of prior diagnosed supersaturation over a time period of 10 min (for our 500 m model, this is 20 time steps). The choice of 10 min is of course somewhat arbitrary, but suffices to examine the sensitivity of N_d to the evolution of supersaturation in the fog. More investigation would be needed to be confident it would generalize from polluted to clean fogs, or to clouds. Thus, in our AD-RAD-DCAT sensitivity simulation, we use activation by adiabatic and radiative cooling as in AD-RAD, together with the following condition.

if (New N_d > Pre-Activation N_d) **then**
  New N_d = Pre-Activation $N_d + \Delta N_{d,\text{Activation}}$
else
  New N_d = Pre-Activation $N_d + \frac{dt}{600} \times \Delta N_{d,\text{Activation}}$
end if

3.5 Only radiative cooling (RAD)

We aim to quantify the relative importance of adiabatic and radiative cooling during the life cycle of fog. By comparing the AD simulation with the AD-RAD simulation, we can quantify the contribution from radiative cooling. However, since these two cooling processes do not result in cloud droplet concentrations that add linearly, in a further simulation labeled "RAD" we remove the adiabatic cooling term from the source of supersaturation and activate only by radiative cooling. We can then compare this simulation with the AD-RAD simulation to understand the relative importance of adiabatic cooling.

3.6 Summary of sensitivity studies

Table 1 shows a brief description of all the simulations used in this study. We aim to provide a direct comparison with the default setup and discuss the importance of aerosol activation via radiative cooling.

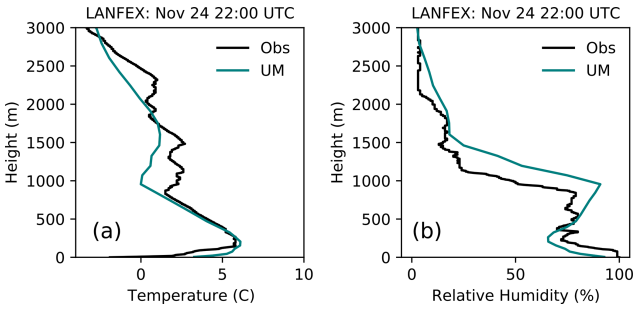

Figure 3. Radiosonde profiles of temperature **(a)** and relative humidity **(b)** from the LANFEX case study at 22:00 UTC. Model results are from the Def-ARG simulation in our 500 m resolution domain.

4 Results

4.1 Evaluation of meteorology during LANFEX IOP1

Radiation fog is formed in stable conditions under clear skies. In Fig. 3 vertical profiles of temperature and relative humidity (RH) at 22:00 UTC are shown from the LANFEX case study. Similarly to the ParisFog radiosonde profiles shown in the companion paper, the soundings are compared with simulated temperature and RH profile in the 500 m model from the Def-ARG simulation. The fog event is associated with a ground level inversion, which extends to around 100 m, the top height of the fog in the model and the observations. Simulated temperature and relative humidity near the surface agree well with the observations. The temperature is within 1° and the RH is within 5 % of the observations. However, higher in the atmosphere (above 1 km), the agreement is relatively poor, with ∼ 2° biases in temperature and 10 % in RH. Fortunately, biases above 1 km do not strongly affect the model performance unless they lead to the formation of cloud layers above the fog. Biases of similar magnitude are also found in the ParisFog cases discussed in the companion paper.

For the LANFEX case, the model produces fog roughly at the correct location in our simulations. In Fig. 4 we show the spatial variation of the grid average N_d and LWC on 24 November. The model results are near the surface, from the AD simulation, in the 500 m resolution domain. There is sufficient fog in the domain for a statistically robust evaluation of the microphysics. Figure S3 shows N_d and LWC in simulation AD-RAD, which has slightly greater coverage of fog, and higher N_d and LWC, than simulation AD. Figure S4 presents the time series of the number of foggy grid boxes at the surface during the ParisFog events, as simulated by the 500 m model for both AD and AD-RAD experiments. The fog coverage is similar between the two simulations, with only minor differences observed on certain days, such as 22 November.

Table 1. Summary of sensitivity experiments conducted in this study. Here, dT/dz refers to the change in temperature with height. In a temperature inversion, dT/dz is > 0. ARG-New denotes whether ARG parameters are updated and "Ad Cool" and "Rad Cool" whether adiabatic and radiative cooling are included, respectively, in the simulations.

Simulation	ARG-New	Ad Cool	Rad Cool	Interception	DCAT
Def-ARG	No	Yes	No	No	No
AD	Yes	Yes	No	No	No
AD-RAD	Yes	Yes	Yes	No	No
AD-RAD-SED	Yes	Yes	Yes	Yes	No
AD-RAD-INV	Yes	if $dT/dz < 0$	Yes	No	No
AD-RAD-DCAT	Yes	Yes	Yes	No	Yes
RAD	Yes	No	Yes	No	No

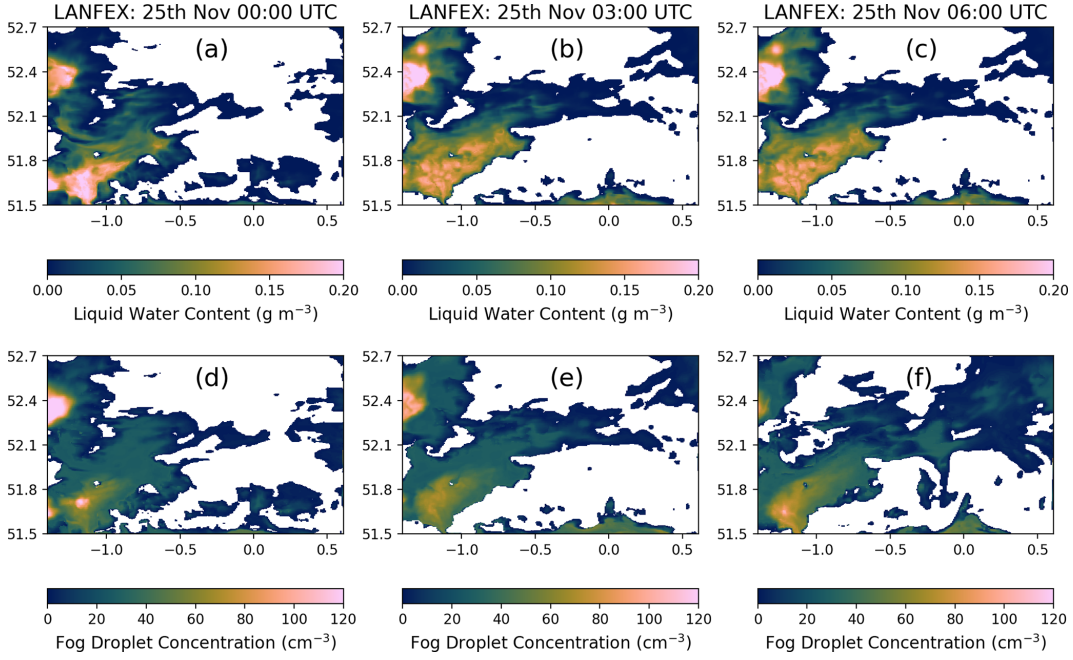

Figure 4. Spatial variation of grid average N_d and LWC on 25 November during the LANFEX field campaign for different times (UTC). We show these properties at 5 m altitude in our 500 m model from simulation AD.

4.2 Comparison of size distributions between ParisFog and LANFEX

In Fig. 5, we show the dry and ambient aerosol size distribution in the AD simulation in our 500 m model, comparing the ParisFog case on 16 November 2011 with the LANFEX case study for 25 November 2014. The ParisFog observations are from the combination of SMPS, WELAS and fog monitor as described in the companion paper. We also plot the fog droplet size spectrum from the observations during the LANFEX case. Solid lines represent the total number concentrations, while dashed lines represent different aerosol modes and the droplet size distribution. We present an average size distribution from the foggy grid boxes near the surface at 03:00 UTC. Foggy grid boxes are those with at least 20 % cloud cover and 0.005 g m^{-3} LWC in that grid box. We also do not include the 20 grid boxes closest to the edges of the domain. These choices are in line with the companion paper and are maintained throughout the manuscript unless otherwise stated. Unfortunately, observations of aerosol sizes are not available for the LANFEX case study; thus we picked a case from ParisFog that had a similar aerosol size distribution. We also show the N_d distribution from the Def-ARG and the AD-RAD simulations. The number concentration of aerosol particles greater than 100 nm in diameter at SIRTA during ParisFog is shown in Ghosh et al. (2025c) Fig. 8. At the time shown in Fig. 5 it is 1550 cm^{-3} while during LANFEX it is 800 cm^{-3}. The higher aerosol number concentrations in ParisFog compared to LANFEX are expected given the contrasting urban and rural locations. Coarse mode aerosol number concentrations are one order of magnitude higher in the LANFEX case than in the ParisFog case, but still two orders of magnitude smaller than the simulated

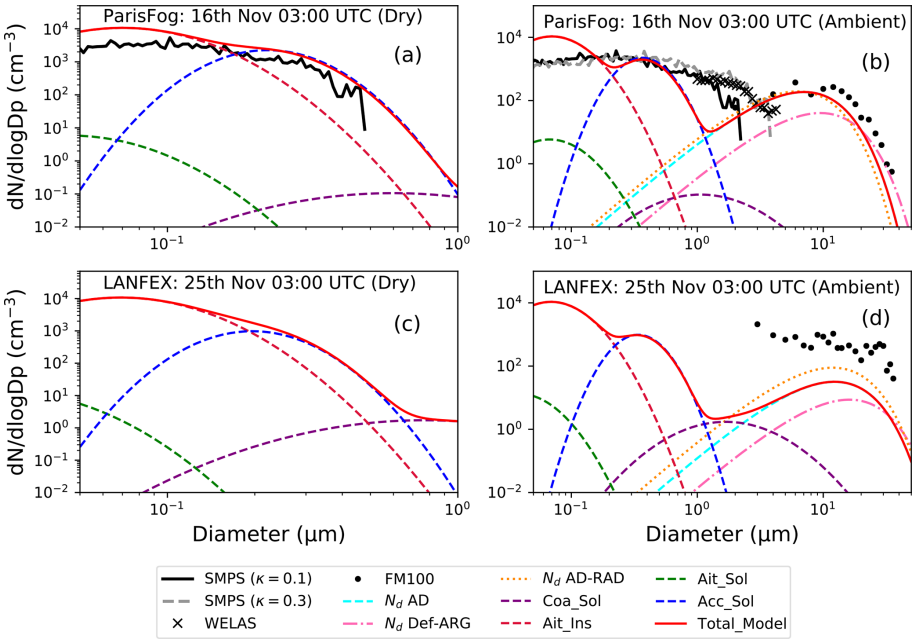

Figure 5. Dry and ambient size distribution of aerosols for the 16 November 2011 ParisFog case **(a, b)** and the 25 November 2014 LANFEX case study **(c, d)** from the AD simulation. The average concentrations in different lognormal modes and the gamma distribution of N_d , near the surface of the foggy grid boxes in the 500 m resolution from the AD simulation, are shown at 03:00 UTC for the two cases. Observations are from the SMPS (ParisFog only), the WELAS (ParisFog only), and the fog monitor (ParisFog at 03:00 UTC and LANFEX from a short measurement at 03:30 UTC, compared to hourly simulation output at 03:00 UTC). The N_d distribution from the Def-ARG and AD-RAD simulations are also shown using pink and orange dashed lines, respectively. The aerosol size distributions from Def-ARG and AD-RAD are similar to AD and are not shown separately.

droplet concentrations, and are hence unlikely to impact the simulated fog. The figure also shows that fog droplets, on average, are lower in concentration and larger for LANFEX than for the ParisFog case (about 10 µm compared to 7 µm), as expected given the lower aerosol concentrations. At 03:00 UTC during the ParisFog case, the droplet size distribution in the AD-RAD simulation changes only marginally compared to the AD simulation. In contrast, for the LANFEX case, N_d is higher in AD-RAD than in AD, and the distribution in AD-RAD shows better agreement with observations, though it still underestimates them. The comparison is discussed further in Sect. 4.3. The increase in N_d in the AD-RAD simulation compared to AD suggests that radiative cooling plays a more significant role in fog development in the LANFEX case.

On 16 November, the observed droplet size distribution is in better agreement with simulation AD and AD-RAD at around 10 µm; however above 30 µm, simulation Def-ARG seems to perform better. However, we show later (Fig. 6b) that N_d on this day is in much better agreement in AD and AD-RAD compared to Def-ARG, despite Def-ARG predicting droplet diameters that are slightly closer to observations. This discrepancy arises mainly because Def-ARG underestimates the LWC, and this LWC bias shifts the gamma distribution used in the model towards larger droplet diameters.

4.3 Time series of fog droplet concentration and liquid water content during ParisFog

In Fig. 6, we demonstrate the performance of the model in simulating N_d during different ParisFog cases from simulations Def-ARG (green), AD (purple), and AD-RAD (orange). We plot the median (solid and dashed lines) and interquartile ranges (shaded regions) from the foggy grid boxes at the surface.

We calculate the normalized mean bias factor (NMBF) and the normalized mean error factor (NMEF), defined as:

$$\mathrm{NMBF}(\overline{M} \geq \overline{O}) = \frac{\sum_i (M_i - O_i)}{\sum_i O_i}$$

$$\mathrm{NMBF}(\overline{M} < \overline{O}) = \frac{\sum_i (M_i - O_i)}{\sum_i M_i}$$

$$\mathrm{NMEF}(\overline{M} \geq \overline{O}) = \frac{\sum_i |M_i - O_i|}{\sum_i O_i}$$

$$\mathrm{NMEF}(\overline{M} < \overline{O}) = \frac{\sum_i |M_i - O_i|}{\sum_i M_i}.$$

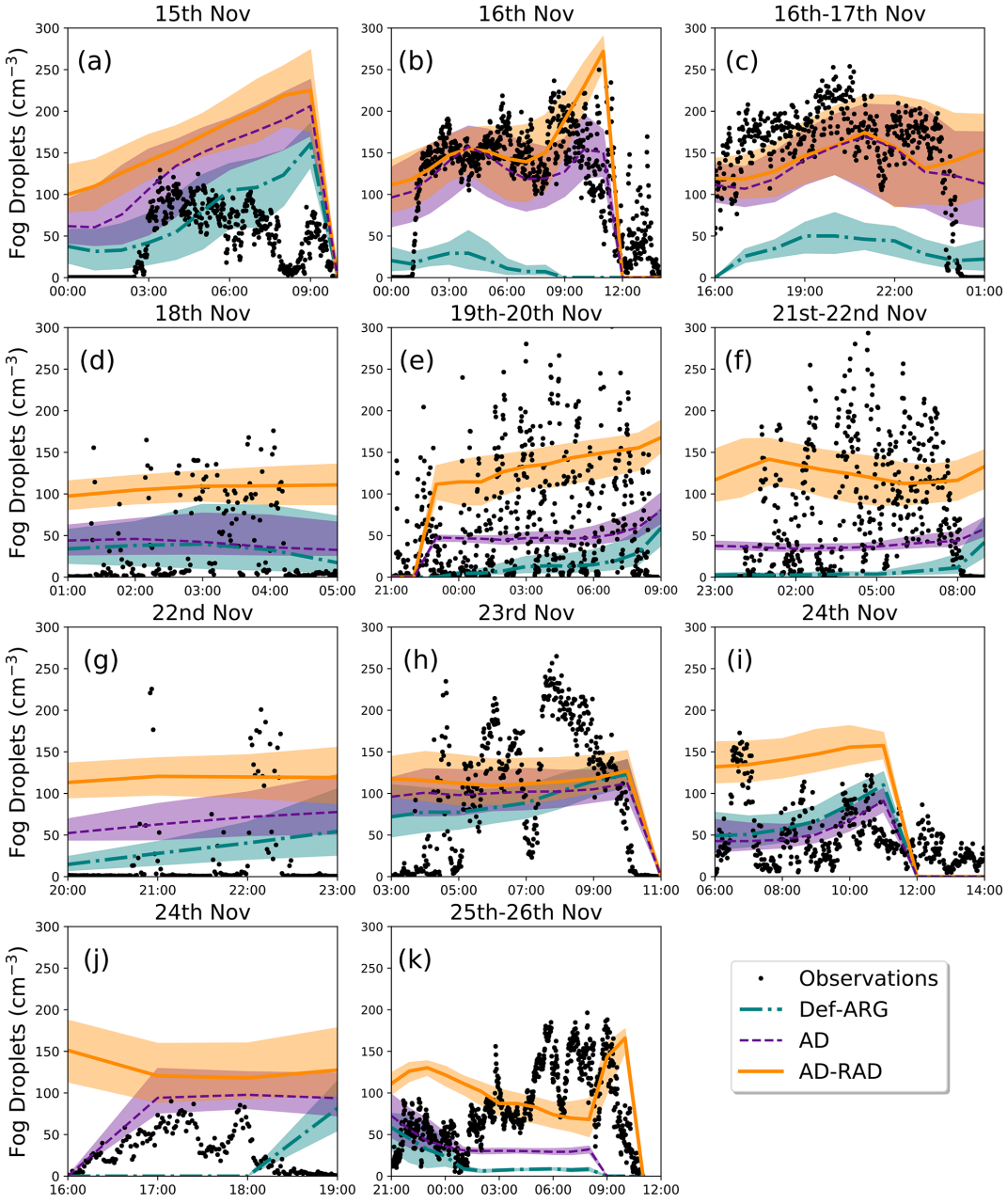

Figure 6. Variation of simulated and observed fog droplet number concentrations as a function of time for different fog events. The results of the 500 m model at 5 m altitude from the simulations Def-ARG, AD, and AD-RAD are compared with observations at the SIRTA observatory (UTC time). Lines represent the median value and the shaded regions represent the interquartile range over the foggy grid boxes.

Here, M_i is the model data, O_i is the observation data, $\overline{M}$ is the model mean, and $\overline{O}$ is the observation mean. NMBF has a range of $-\infty$ to $+\infty$, and NMEF has a range of 0 to $+\infty$. We report NMBF and NMEF for all fog cases in Tables S1 and S2 in the Supplement and use them as a tool to compare the model performance among different simulations.

In simulation AD-RAD, the N_d are higher than in simulation AD because of droplet activation via radiative cooling. The difference in N_d is about 50–100 cm^{-3} for all fog events except those on 16 November. For the fog cases on 16 November, radiative cooling is unimportant and simulations AD and AD-RAD behave similarly. Otherwise, the model bias increases for all the fog cases. For example, on 15, 18, and 24 November (first case) (Fig. 6a, d and i), AD-RAD tends to overestimate N_d and the NMBF (NMEF) change from 1.97, 0.34, −0.17 (2.02, 0.89, 0.64) in AD to 2.67, 2.55, 1.18 (2.72, 2.55, 1.61) in AD-RAD.

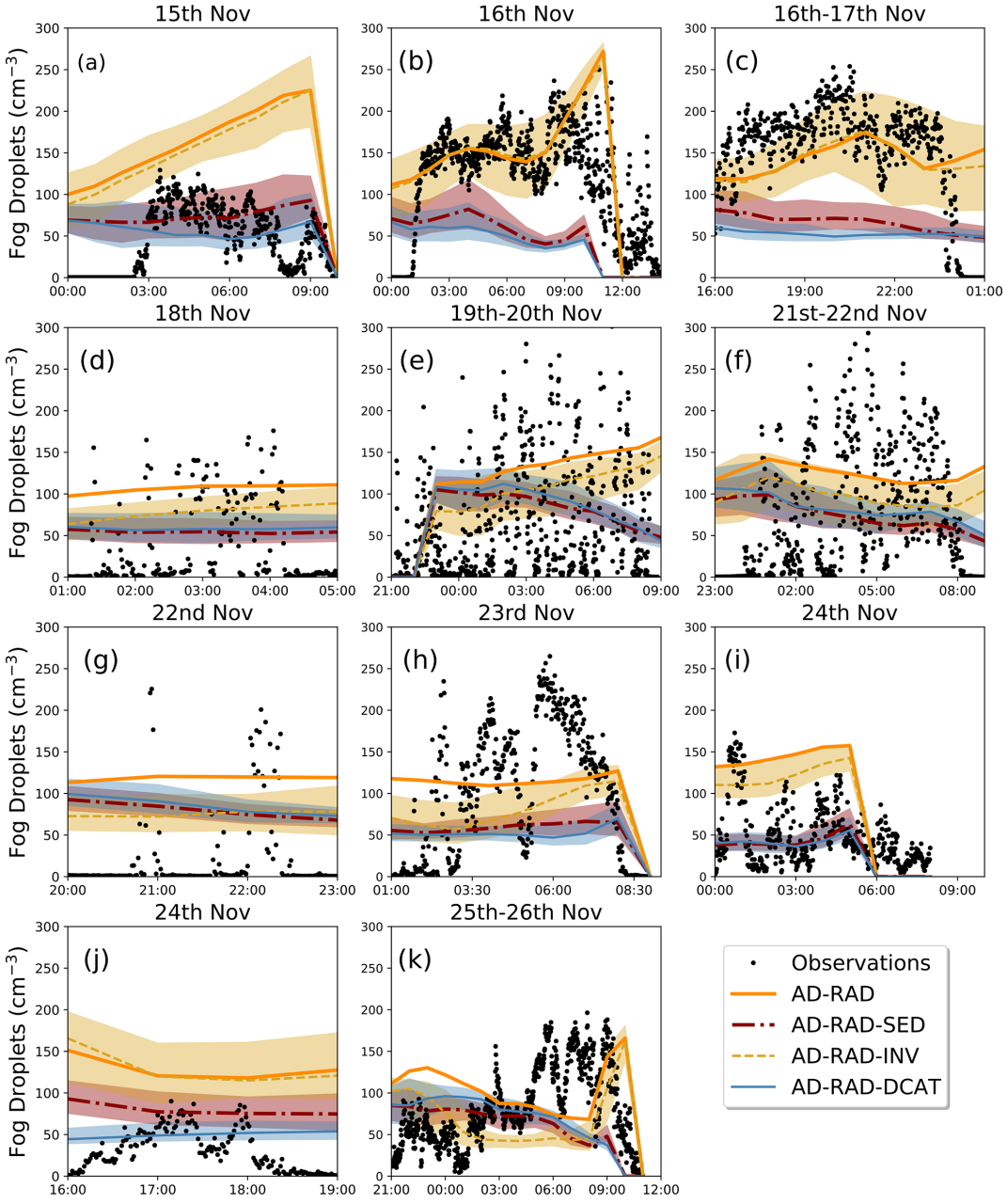

Figure 7. Variation of simulated and observed fog droplet concentration as a function of time for different fog events. The median and interquartile range from the 500 m model at 5 m altitude from the simulations AD-RAD, AD-RAD-SED, AD-RAD-INV, and AD-RAD-DCAT are compared with observations at the SIRTA observatory (UTC time). Lines represent the median value and the shaded regions represent the interquartile range over the foggy grid boxes.

In Fig. 7, we show time series of N_d for ParisFog cases for our sensitivity studies: AD-RAD-SED, AD-RAD-INV, and AD-RAD-DCAT. We show median (solid and dashed lines) and interquartile range (shaded region) from the foggy grid boxes at the surface in the 500 m model. We also show the median N_d from the AD-RAD simulation for ease of comparison. We apply a LWC threshold of 0.005 g m^{-3} and a cloud fraction threshold of 20 % to define a grid box as "foggy"; the fog event is defined as the period for which over 1000 grid boxes in the model domain are "foggy".

In simulation AD-RAD-SED (red), increasing the sedimentation rate at the lowest model level to represent the interception of fog droplets by trees and buildings substantially reduces the droplet number concentrations (compared to AD-RAD) during all fog events. In this simulation, the overestimation of N_d in AD-RAD is reduced and the model

agrees better with the observations. For the 16 November cases, the model is now biased low (the NMBF is −1.43 and −1.10). For other fog cases, the biases have been reduced compared to AD-RAD. For example, for the first fog case on 24 November, the NMEF is now −0.51 compared to 1.18 in AD-RAD. Compared to simulation AD, performance improvement is also found in 6 fog cases out of 11. For example, in the 15, 19, and 26 November cases, the model is in better agreement with the observation in simulation AD-RAD-SED compared to simulation AD. The NMBF (NMEF) changes from 2.67, 0.35, 0.31 (2.72, 0.99, 0.71) to 0.67, −0.20, −0.27 (0.87, 0.81, 0.76). This simulation supports the findings of other studies (e.g., Mazoyer et al., 2017) that fog deposition is an important physical process that affects the droplet budget, although we cannot be sure that our crude modification accurately simulates real losses due to interception.

In simulation AD-RAD-INV (yellow), we prevent activation in temperature inversions (in addition to changes in AD-RAD). Similarly to the AD-RAD-SED simulation, we find that simulation AD-RAD-INV is also a significant improvement over the AD-RAD simulation, though not (for the majority of cases) over the AD simulation. Our hypothesis leads to minimal changes (compare the yellow solid lines with 15, 16 (both events), and 24 November (second event). However, for other fog cases, the changes in N_d are significant. Compared to simulation AD-RAD, 10 out of 11 fog cases have lower biases.

The AD-RAD-DCAT simulation (blue) introduces the droplet concentration adjustment timescale, testing the sensitivity to several physical processes and model artifacts that affect the droplet budget in the fog. This simulation performs similarly to AD-RAD-SED and improves the model performance compared to AD-RAD for most cases; when compared to AD it improves model performance for a slim majority of cases (6 out of 11). For example, on 15, 18, and 24 November, the model now agrees well with the observation compared to AD-RAD. However, on 16 November, there is a factor of 2 underestimation. This test suggests that improving the representation of physical processes like collision-coalescence, or the hygroscopic growth of unactivated haze aerosols, may be important to improve fog simulation in climate and weather models.

There are other possible explanations for the overestimation of droplet concentrations when radiative cooling is included in the aerosol activation mechanism we do not test. For example, Boutle et al. (2018) suggested that in their UKV simulation, which is similar to ours but without interactive aerosols, their radiative cooling rates could be too high. There may also be a positive feedback mechanism that could exacerbate the problem (Boutle et al., 2018): more, smaller droplets can absorb radiation from the surface more efficiently leading to more radiative cooling, which may then result in more activation.

In Fig. 8, we compare the time series of in-fog liquid water content in foggy grid boxes (LWC) with observations. Figure 8a–k denote different ParisFog cases. We show median and interquartile ranges (using lines and shaded regions) from the foggy grid boxes at the surface in our Def-ARG, AD, and AD-RAD simulations. In-fog liquid water content is calculated by dividing the grid average LWC by the cloud cover. Since low LWC grid boxes also tend to have a low cloud fraction, the minimum LWC in the time series is the LWC threshold for a box to be "foggy" of $0.005\,g\,m^{-3}$ divided by the cloud fraction threshold of 20 %. The inset histograms of in-fog LWC show the variability between grid boxes at a representative time during each fog event from simulation AD. On 22 and 23 November, the LWC in the AD-RAD simulation closely resembles that of the Def-ARG and AD simulations. As in the companion paper and as expected from simulations of liquid water path evaluated in other studies (Boutle et al., 2022), the model has relatively little skill in representing the trends in LWC during the observed fog events and the AD simulation usually performs better than AD-RAD. The interquartile ranges and histograms suggest LWC is more spatially heterogeneous in the simulations than N_d, complicating the interpretation of the comparison of the point measurements with the domain-median simulated LWC. Generally, LWC tends to increase when radiative cooling is included in aerosol activation in the AD-RAD simulation, except during the first fog event on 16 November (Fig. 8b). LWC is often over-predicted during the early stages of the fog, for example on 15, 21, and 25 November (Fig. 8a, f and k). The mechanisms for the aerosol–fog interactions we simulate are likely similar to those discussed in the companion paper.

Figure S5 shows the LWC time series for the AD-RAD-SED, AD-RAD-INV, and AD-RAD-DCAT simulations. Unlike in the case of the N_d time series, AD-RAD-DCAT and AD-RAD-SED sometimes differ substantially, with AD-RAD-SED producing LWC a factor of two lower than AD-RAD-DCAT on 18, 19, and 21 November. Including a representation of droplet interception significantly reduces the overestimate of LWC near the surface compared to AD-RAD in these three thin fogs, as well as also improving N_d. However, AD-RAD-DCAT is relatively similar to AD-RAD. This difference between AD-RAD-DCAT and AD-RAD-SED is expected, as increasing sedimentation removes the liquid water mass while introducing DCAT only influences the LWC via aerosol–fog interactions. Despite the improved mean LWC in simulation AD-RAD-SED compared to AD-RAD, none of the simulations substantially improved on the poor skill of simulation AD in representing LWC trends during the fogs.

In summary, we find that incorporating radiative cooling as a source of supersaturation leads to increased surface droplet concentrations across all fog events. NMBF and NMEF are presented for all fog cases in Supplement Tables S1 and S2. On certain days, such as 16 November, the relative increase

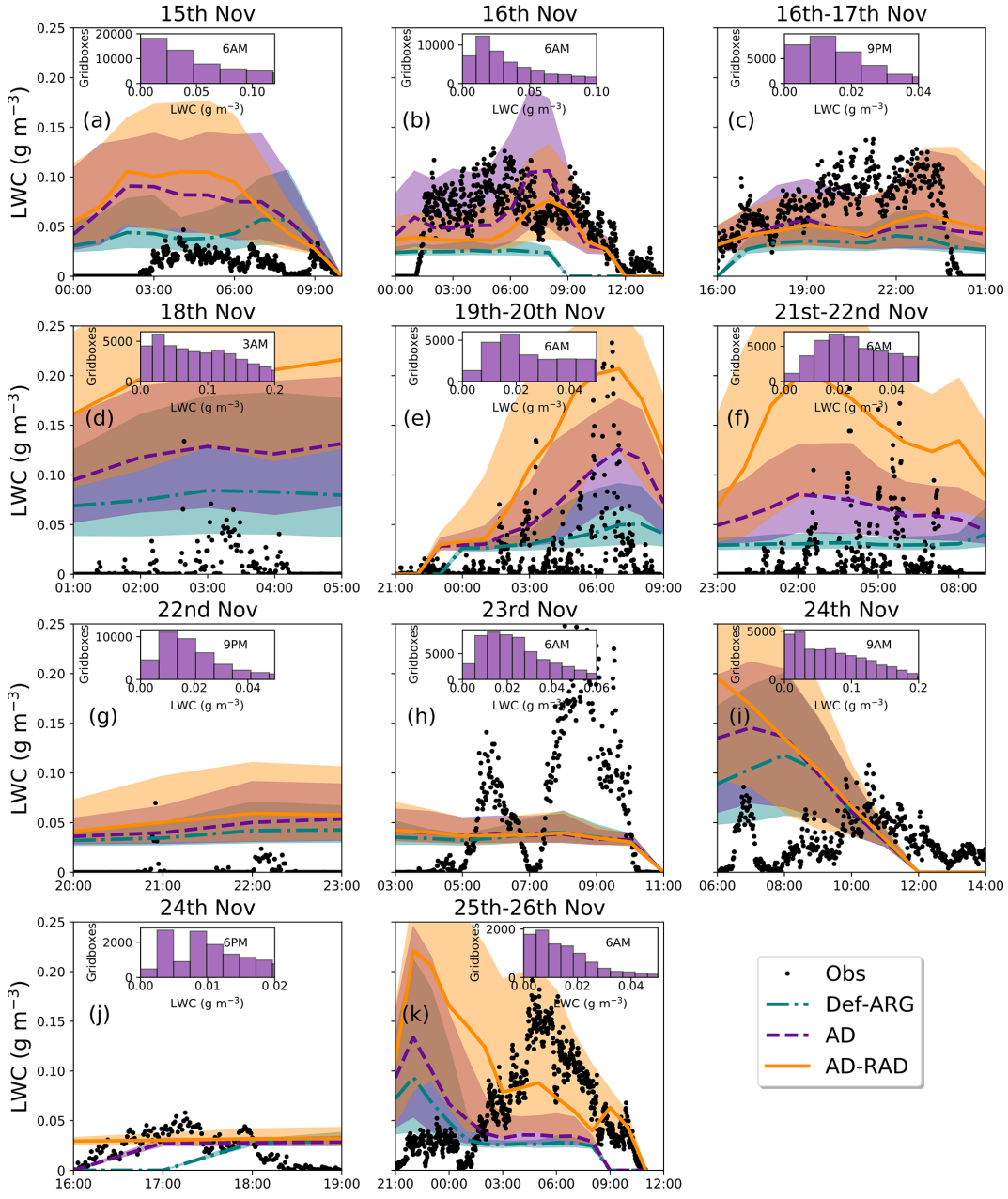

Figure 8. Variation of simulated and observed liquid water content as a function of time for different fog events. The results of the 500 m model at 5 m altitude from the simulations Def-ARG, AD, and AD-RAD are compared with observations at the SIRTA observatory (UTC time). The solid and dashed lines represent the median values and the shaded regions represent the interquartile ranges over the foggy grid boxes. The inset plots show histogram of in-fog liquid water content at different times of the fog events from the AD simulation. The minimum LWC visible in the plots of around 0.025 g m^{-3} is due to the thresholds for defining grid boxes as foggy, as described in the text.

in N_d is minimal at this altitude for the majority of the fog, highlighting the dominant role of adiabatic cooling. In contrast, on days like 26 November, we find a substantial increase in N_d, indicating a stronger contribution from radiative cooling, bringing the model outputs into better agreement with observations. Consistent with the findings of the companion paper, the LWC shows a lower sensitivity to changes in aerosol activation than N_d, and the model exhibits limited skill in capturing the time variation of observed surface LWC across different simulation configurations.

4.4 Liquid water path

We are also able to evaluate liquid water path (LWP), which gives additional insight into the behavior of the fog at higher altitudes. For LANFEX, Fig. 9a shows LWP time series from

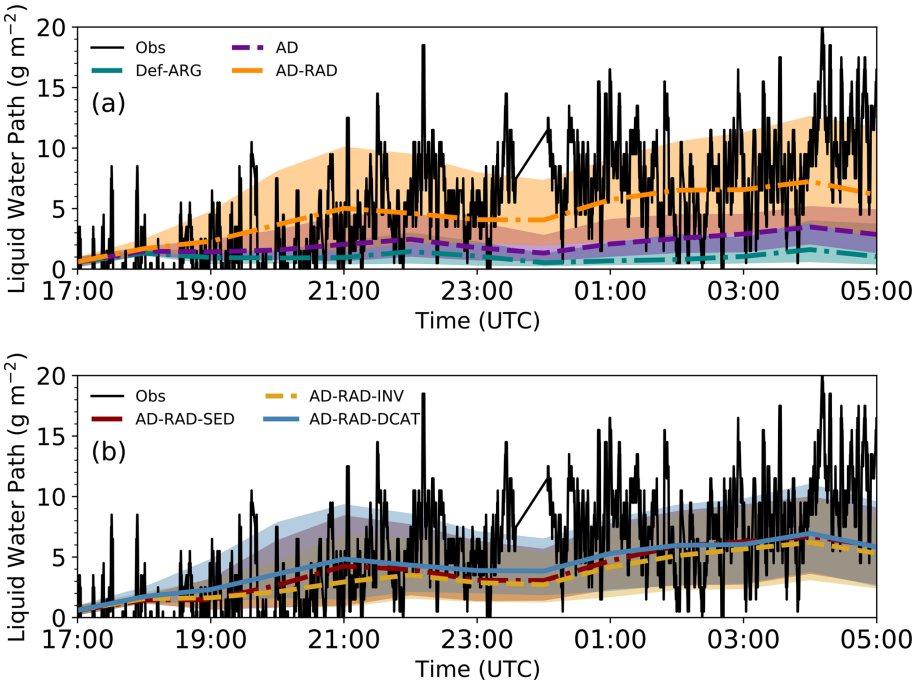

Figure 9. Time series of liquid water path during the LANFEX case study for different simulations. **(a)** Def-ARG, AD, and AD-RAD. **(b)** AD-RAD-SED, AD-RAD-INV, and AD-RAD-DCAT.

the microwave radiometer observations and simulations Def-ARG, AD, and AD-RAD and Fig. 9b shows AD-RAD-SED, AD-RAD-INV, and AD-RAD-DCAT. To calculate LWP in simulated fog while excluding simulated clouds, we select the foggy grid boxes at the surface and calculate the LWP in those columns. As the radiometer would include LWP contributions from clouds above fog, we also allow these to contribute in the simulations. Then we calculate the median and interquartile range, and plot them as solid (and dashed) lines and shaded regions for different simulations. The Def-ARG simulation significantly underestimates the LWP during the lifetime of the fog. The AD simulation, which uses the updated ARG scheme, reduces the bias but still shows a discrepancy greater than a factor of 3 most of the time. However, despite the overestimated surface LWC we described in Sect. 4.3, the inclusion of radiative cooling as a source of supersaturation in the AD-RAD simulation substantially improves the model's performance, capturing the early stages of the fog within 50 % of observations, but then converging to a steady mean LWP after 21:00 UTC (around 7 g m^{-2}, similar to the observations). Figure 9 is similar to Fig. 4b of Vié et al. (2024) and Fig. 1 of Boutle et al. (2022). Our AD-RAD simulation is in comparably good agreement with the best performing simulations in the intercomparison. In contrast to LWC in the ParisFog cases, the trend in LWP during the fog is also in good agreement with the observations. In simulations AD-RAD-SED, AD-RAD-INV, and AD-RAD-DCAT, the model performance in simulating the LWP is slightly underestimated, but better than simulation AD and similar to the DT + QC simulation of Vié et al. (2024). The underestimate mirrors the lower N_d and LWC in these simulations compared to AD-RAD. In Fig. S6 we plot the time series of LWP for the ParisFog cases. The AD and AD-RAD simulations are mostly correct in determining whether fog events have low or high LWP (below or above 25 g m^{-2}). However, the agreement with observations during any given fog event is mixed and our conclusion based on LANFEX that AD-RAD performs better than Def-ARG or AD is only true in about half of the fog events.

4.5 Vertical structure of fog

We show simulated vertical profiles of N_d in Fig. 10 with observations from the tethered balloon during LANFEX IOP1. In our 500 m resolution model, we use the following algorithm to select grid cells to include in the vertical profile.

1. Select all foggy grid boxes at the surface level.

2. To define the fog top, move up the columns that correspond to these grid boxes until fewer than 1000 still contain fog.

3. Calculate median fog properties from columns in which the surface grid box contains fog, starting at the surface and moving upwards. For example, in a hypothetical case where 20 000 surface grid boxes are foggy, 15 000 of these also contain fog at model level 2, 8000 of these contain fog at level 3, and 500 at level 4,

the median is calculated over all of these grid boxes for levels 1–3 inclusive.

We plot the median and interquartile ranges of N_d (shown by solid lines and shaded regions) at different model levels from the Def-ARG, AD and AD-RAD simulations. The top panel (Fig. 10a–c) show the vertical profile at different times during the LANFEX case, and other subplots show ParisFog cases.

During the LANFEX case, observations (shown in black solid and dotted lines) indicate a variable fog top height ranging from 50 to 90 m at different times. In the model, the bottom six levels are centered at 5, 22, 45, 75, 112, and 155 m. In simulations AD and AD-RAD, fog extends up to 75 m (the boundary between the 45 and 112 m levels). Above this level, little or no fog is present in the model.

For this case, the Def-ARG simulation consistently underestimates N_d throughout the vertical profile, though its low fog top height at 23:00 UTC is a better match to observations than AD or AD-RAD. Overall simulation AD seems in better agreement with the observations: the fog top height matches locations where $N_d > 20\,cm^{-3}$ and LWC (Fig. 11) is greater than $0.05\,g\,m^{-3}$ within one model level at 23:00 and 00:00 UTC. However, Fig, 11 suggests the fog top is one level too high in both AD and AD-RAD at 03:00 UTC. Moreover, sometimes the N_d is underestimated (during the mature stage of the fog, on 25 November at 03:00 UTC around 20–30 m altitude, for example). As was evident in the time series plots, the inclusion of radiative cooling leads to a moderate overprediction of N_d. On average, we simulate about $70\,cm^{-3}$ droplets in AD-RAD, which is within a factor of two of the observations,similar to Poku et al. (2021) and the LIMA simulation of Vié et al. (2024). Figure 4 of the model intercomparison study by Boutle et al. (2022) shows the vertical profile of N_d simulated by several LES models. Some of these have radiative cooling included in aerosol activation, some do not. In their "high" aerosol cases (which best matches our simulated aerosols), N_d is also usually overestimated by around a factor of 2. For ParisFog, we do not have observations for vertical structure, though Mazoyer et al. (2019) comment that the fog top at SIRTA on 18, 20, 22, and 23 November is below 18 m altitude. Our simulations predict much higher fog top heights on these days. This apparent discrepancy may be mainly due to our selection method, which is designed to select as much fog as possible; it also seems likely from the brightness temperatures shown in Fig. 3 of the companion paper that fog elsewhere in our model domain is more developed than it is at SIRTA, otherwise it likely would not be detected by the satellite. Even in simulations, the simulated fog top heights differ substantially between fog events, ranging from 45 m on 26 November to over 500 m on 23 November. The difference in fog top height between AD and AD-RAD is small on some days (e.g., 16, 20, and 22 November) but significantly larger on others (e.g., 18, 23, and 26 November). However, defining a fog top height is not straightforward. In Fig. S7, we show the vertical profile of number of foggy grid boxes from simulations AD and AD-RAD at 03:00 UTC on 16, 18, and 23 November. For the 18 and 23 November cases, the differences in fog top height arise due to the threshold of 1000 grid boxes we use in this paper. If we instead apply a threshold of at least 10 % foggy grid boxes (6760), the fog top height becomes consistent between AD and AD-RAD: 150 m for 18 November and 280 m for 23 November. However, applying the same threshold to the 16 November case results in different fog top heights: 150 m for AD and 200 m for AD-RAD. Therefore, we believe that any differences (mostly one model level) in fog top height between AD and AD-RAD are primarily due to the choice of threshold.

In Fig. S8, we show vertical profiles of N_d for the AD-RAD-SED, AD-RAD-INV, and AD-RAD-DCAT simulations. For the LANFEX case, although the vertical structure is complex, the profile simulated in AD-RAD-INV shows better agreement with observations while the other two sensitivity studies closely resemble AD-RAD. The differences in N_d at the surface are substantial across all simulations. In the ParisFog cases, the variations among sensitivity studies are much larger at all model levels.

We show vertical profiles of LWC in Fig. 11 in the 500 m resolution model from different sensitivity simulations, similar to Fig. 10. The top panel shows the LANFEX case and other subplots are for ParisFog events. Our changes are designed to improve N_d in the model but they also affect the LWC through aerosol–fog interactions (as discussed in the companion paper). Contrary to the vertical N_d profiles, both simulations AD and AD-RAD are in reasonably good agreement with the LANFEX observations, but there are balloon observations (dotted black line) showing higher fluctuations of LWC near the surface and also at higher altitude. In both model and observations, N_d vertical profiles are correlated to LWC vertical profiles but the correlation is relatively weak. Hence, as also demonstrated by Vié et al. (2024), rather than assuming a perfect correlation (as done in a single-moment microphysics scheme), it is important to use the double-moment cloud microphysics scheme in the model to accurately capture the mean behavior in the vertical profile of fog microphysical properties; however, it is likely that neither single- nor double-moment bulk microphysics can perfectly represent the variability in these profiles. We show similar profiles for the other simulations in Fig. S9.

4.6 Comparison of radiative and adiabatic cooling rates

In Fig. 12, we show the vertical profiles of the radiative cooling rate in the AD-RAD simulation. Figure 12a shows LANFEX IOP1, while Fig. 12b–i show different ParisFog cases. The radiative cooling rates shown in the figure are the mean values from all foggy grid boxes, selected in the vertical as in Fig. 10. An additional color bar shows the updraft velocities that would give cooling rates equal to the simulated radiative

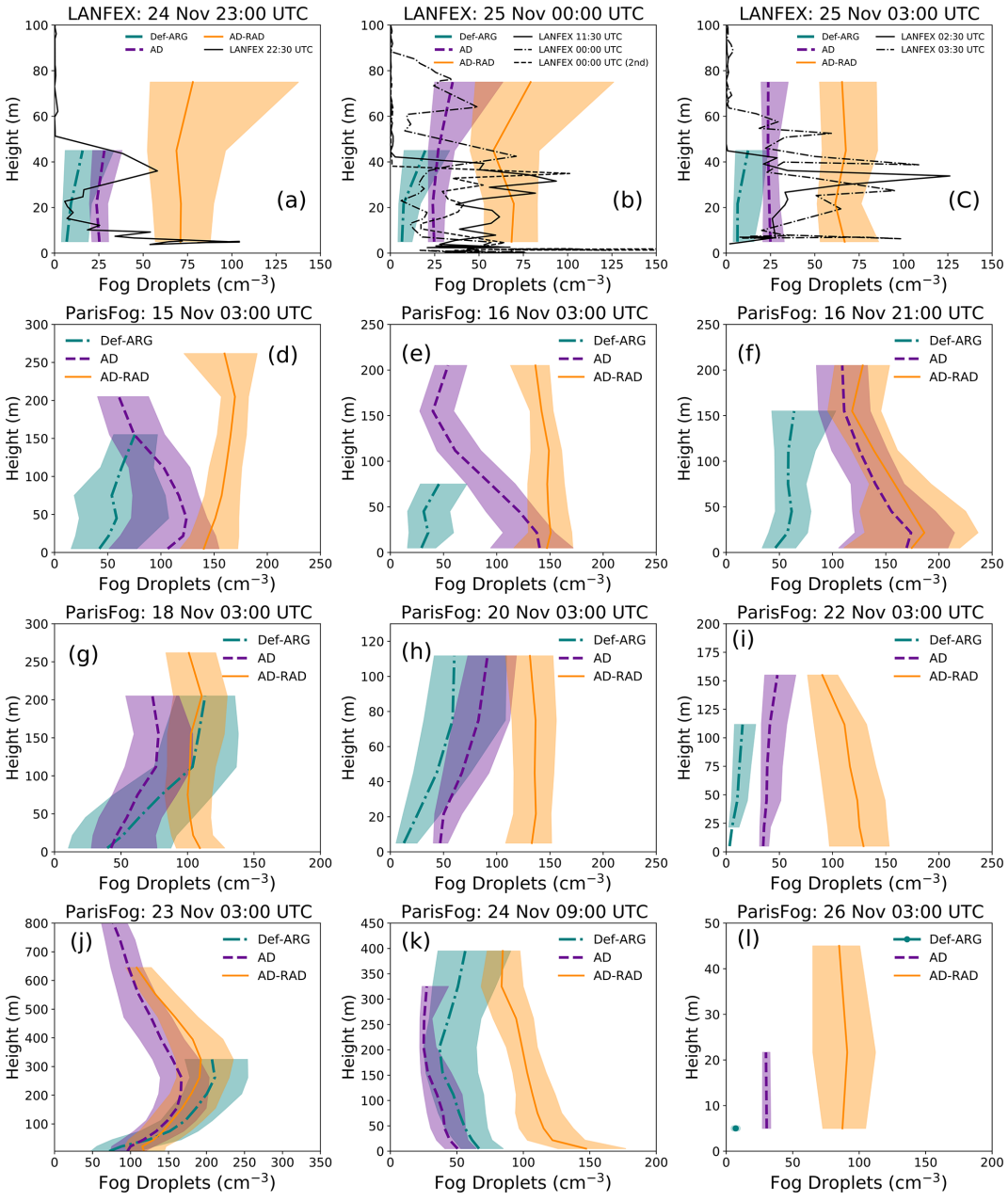

Figure 10. Vertical Profiles of N_d from the LANFEX case study and different days of the ParisFog case study. The results of the 500 m model for Def-ARG, AD, and AD-RAD simulations are shown. Observations during LANFEX are from the fog monitor on the tethered balloon. Note the different y axis scales of the different subfigures, reflecting the substantial variability in fog top height between fog cases.

cooling rates, calculated assuming a temperature lapse rate of 6.5 K km^{-1} as in Boutle et al. (2018).

The radiative cooling rate varies with time and is mostly between 0 and 2.0 K h^{-1} near the surface. Equivalent updraft speeds range from 0–0.08 m s^{-1}. The low equivalent updraft speeds also support the conclusion of Boutle et al. (2018) that a minimum updraft speed of 0.1 m s^{-1} is too high and will artificially inflate simulated droplet concentrations in radiation fog. Cooling rates exhibit substantial variation both within and between fog cases both at the surface and at higher altitudes near the fog top. Although cooling rates are much higher near the fog top (similar to Boutle et al., 2018), activation may be suppressed near the fog top after the time of fog onset. This is because the elevated LWC near the fog top in a well-developed fog (Figs. 11 and S11) can act as a condensation sink, thereby suppressing supersaturation near the fog top (Figs. 10 and S12). In Figs. S10 and S11, we show the vertical profile of N_d and LWC as a function of time

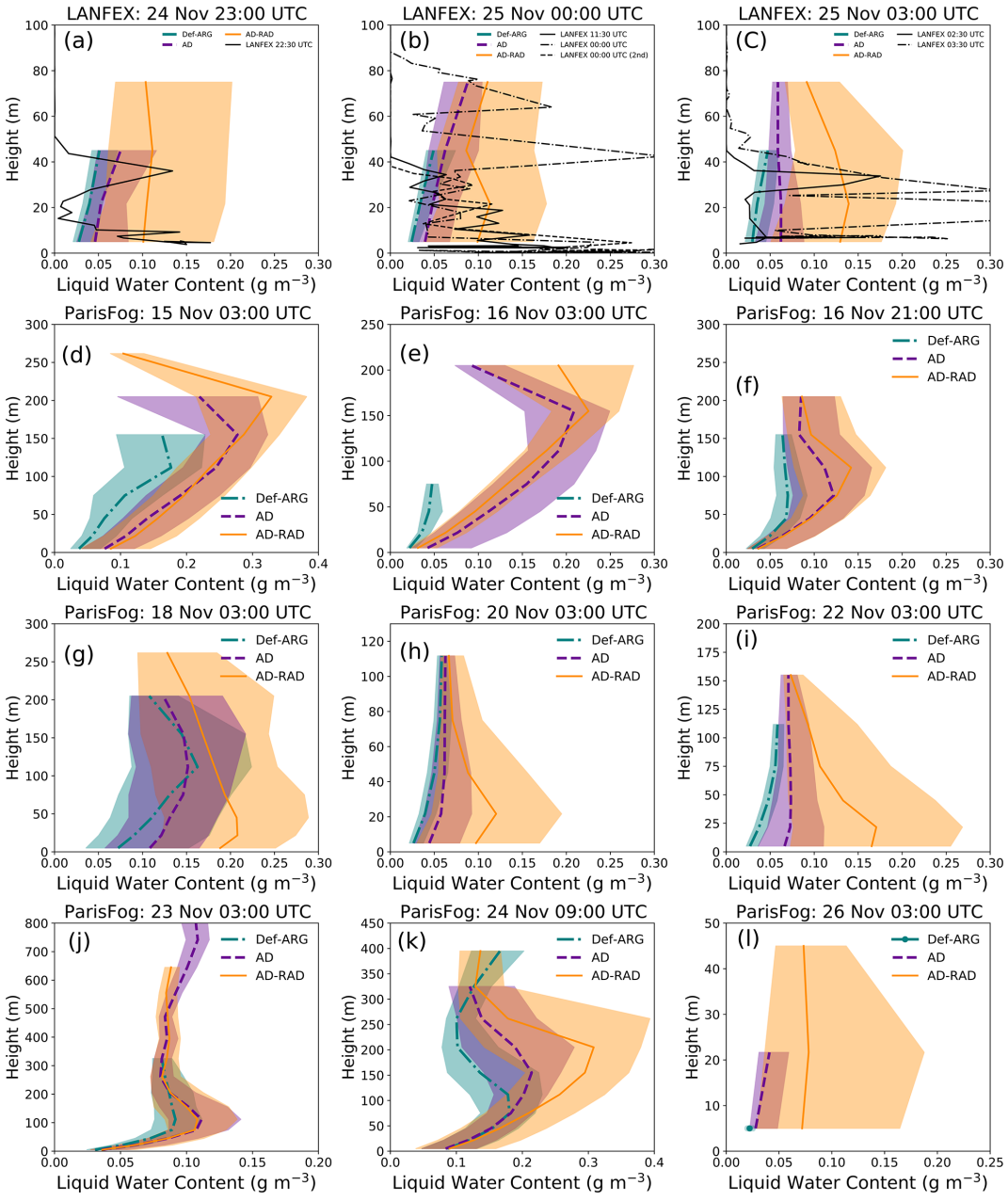

Figure 11. Vertical Profiles of LWC from the LANFEX case study and different days of the ParisFog case study. The results of the 500 m model for Def-ARG, AD, and AD-RAD simulations are shown here. Observations during LANFEX are from the fog monitor on the tethered balloon. Note the different y axis scales of the different subfigures, reflecting the substantial variability in fog top height between fog cases.

through the fog events. With time, the height of the maximum LWC increases for some fog cases, but not all. For some ParisFog cases, the LWC increases with height until the maximum LWC is reached, demonstrating that a subset of the 11 ParisFog events we study are adiabatic fog (15, 16, 23, and 24 November) while others are clearly not.

In Fig. 13 we show the spatial variation of the radiative cooling rate in the model at a representative time for LANFEX and two ParisFog cases. The spatial variations exceed a factor of two across our relatively small and – while not spatially homogeneous, at least not mountainous – model domains. The high variability of the radiative cooling rate suggests that using a constant minimum updraft speed is probably a poor proxy for radiative cooling in simulations of aerosol activation in fog.

To understand the relative importance of adiabatic and radiative cooling in droplet activation in these fog cases, we compared droplet concentrations in the AD-RAD simulation

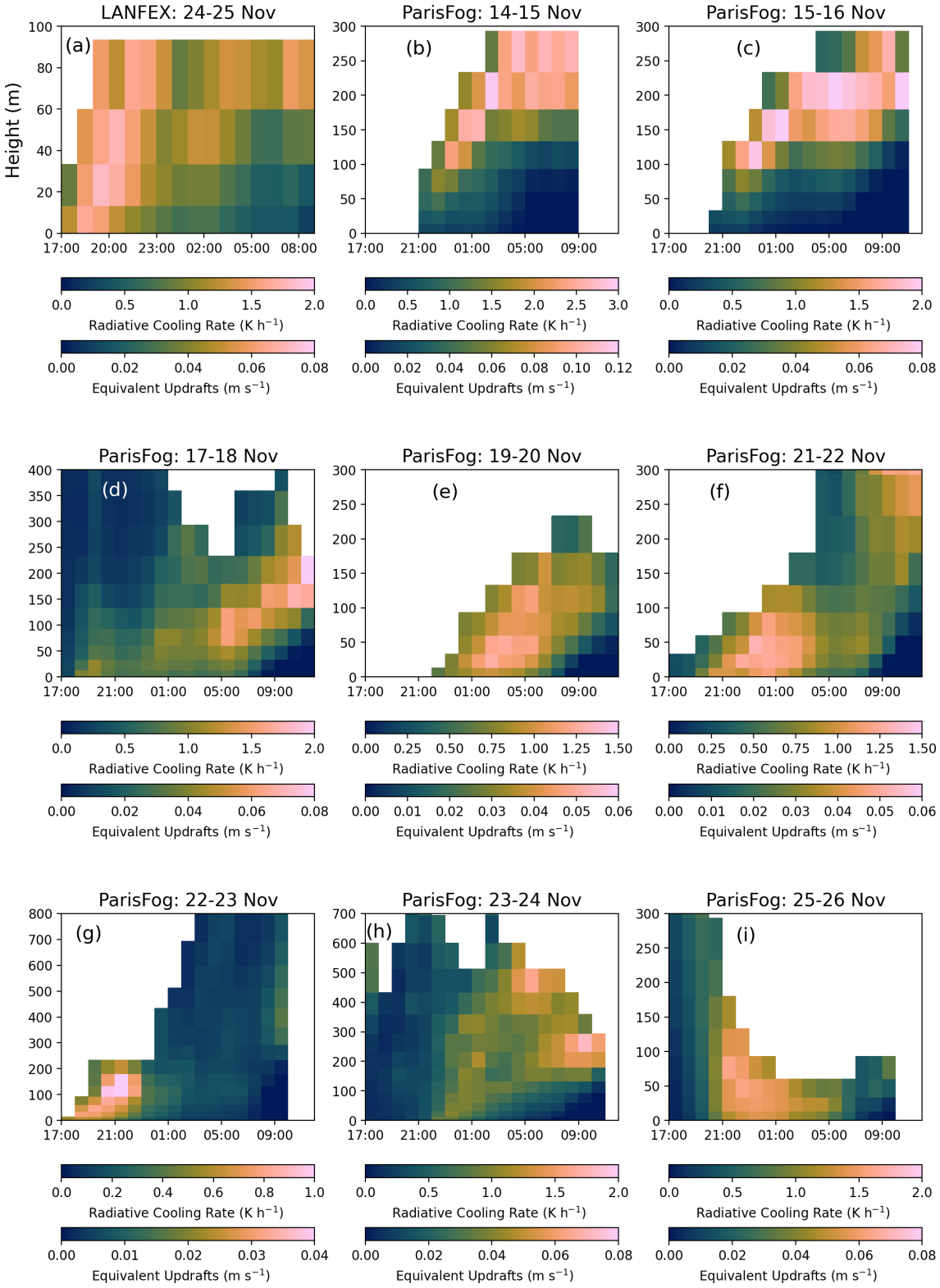

Figure 12. Vertical profile of radiative cooling rate in our 500 m resolution AD-RAD simulation, as a function of time (UTC). Subfigure **(a)** represents the fog event from the LANFEX case, and subfigures **(b)**–**(i)** represent different ParisFog cases. The median cooling rates of all foggy grid boxes (at the surface and their vertical column following the algorithm described earlier) are plotted. Equivalent updrafts (assuming a 6.5 K km^{-1} temperature lapse rate) are also shown in the additional color bar.

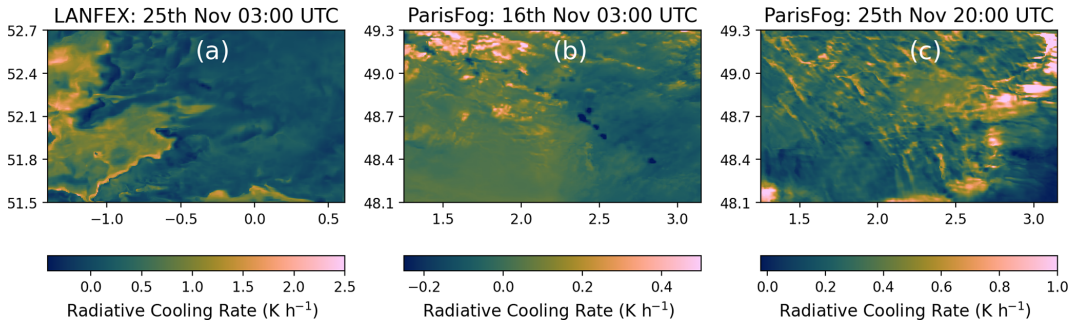

Figure 13. Spatial variation of radiative cooling rate at the surface from simulation AD-RAD of the 500 m model for the LANFEX case **(a)** and two ParisFog cases **(b, c)**.

with those in the AD and RAD simulations. Simulation AD-RAD has both cooling terms, whereas simulation AD and RAD have only adiabatic and radiative cooling terms, respectively. Therefore the marginal contributions of the two mechanisms are as follows:

$$\text{Radiative Cooling Contribution} = \frac{N_\mathrm{d}(\text{AD-RAD}) - N_\mathrm{d}(\text{AD})}{N_\mathrm{d}(\text{AD-RAD})}$$

$$\text{Adiabatic Cooling Contribution} = \frac{N_\mathrm{d}(\text{AD-RAD}) - N_\mathrm{d}(\text{RAD})}{N_\mathrm{d}(\text{AD-RAD})}.$$

When calculating these contributions, we select the foggy grid boxes in the AD-RAD simulation and use the same locations in the other two simulations, irrespective of the presence of fog in that area. The resulting contributions are shown in Fig. 14. The two marginal contributions generally do not add to 100 %, as expected, because some aerosol particles can be activated by either cooling source (so the marginal contributions sometimes amount to more than 100 %), while other aerosol particles require the sum of the cooling rates to activate (so the marginal contributions sometimes sum to less than 100 %).

We find the marginal contribution of radiative cooling to aerosol activation is substantial, and indeed dominant in the majority of ParisFog cases and the LANFEX case we study here. A major caveat is that results are likely influenced to some extent by the overestimation of N_d in simulation AD-RAD. Qualitatively, however, this result supports the findings of Poku et al. (2021) that radiative cooling is important. In the LANFEX case, we find the contribution of radiative cooling ranges from 60 %–70 %. However, for the ParisFog cases, simulated adiabatic cooling is frequently also important, even in radiation fog, and the relative contributions of radiative and adiabatic cooling have large inter- and intrafog variability for both sources. Among the ParisFog cases, on 19, 21, 23, 24 (first event), and 26 November, radiative cooling is the dominant source, with contributions ranging from 60 %–80 %. During fog events on 15 November (starts at 03:00 UTC) and 16 November (both), adiabatic cooling is the dominant source, with a marginal contribution maximum up to 80 %. This is most likely due to substantially lower radiative cooling rates below the fog top during these fog events compared to other cases (see Fig. 12). The radiative cooling rate at the surface is approximately 0.2 K h^{-1}, corresponding to an equivalent updraft of about 0.01 m s^{-1}. In contrast, during the 26 November fog event (where radiative cooling is the dominant driver of aerosol activation) the cooling rate is significantly higher, around 1.5 K h^{-1} (equivalent updraft of 0.06 m s^{-1}). Although the peak cooling rates on 15 and 16 November are higher and occur near the fog top (likely due to a slightly elevated inversion height, as shown in Fig. 5 of the companion paper), it is possible that most droplet activation during these cases (after the initial fog onset) still occurs below the fog top, where the liquid water content (LWC) is lower (Figs. 11, and S11). This could explain why radiative cooling plays a less significant role in droplet activation during the 15 and 16 November fog events. On 16 November, after 06:00 UTC, the fog top radiative cooling rates increase compared to those at fog onset, perhaps enhancing droplet activation at lower altitudes and leading to increased droplet concentrations near the surface, as shown in Fig. 6b. For the 22 November late evening fog case, both cooling sources are equally important but vary during the fog life cycle. In radiation fogs, we generally expect that the fog layer is initially thin and radiative cooling is dominant. With time, the fog layer thickens, and mixing within the fog layer makes the fog more adiabatic, and updraft speeds increase; so radiative cooling becomes less important (Boutle et al., 2018). In many of the fog cases (e.g., ParisFog: 15, 22, 24 November and the LANFEX case), but not all, we find that the contribution from radiative cooling is more important during the initial phases of fog development. As the fog layer thickens, the contribution decreases as the fog becomes more adiabatic. However, unsurprisingly, in these weather prediction simulations, the effect is harder to disentangle from case-by-case variability than in a more idealized LES simulation.

5 Discussion and conclusion

In this study, we simulate radiation fog during the ParisFog and LANFEX field campaigns using 500 m resolution

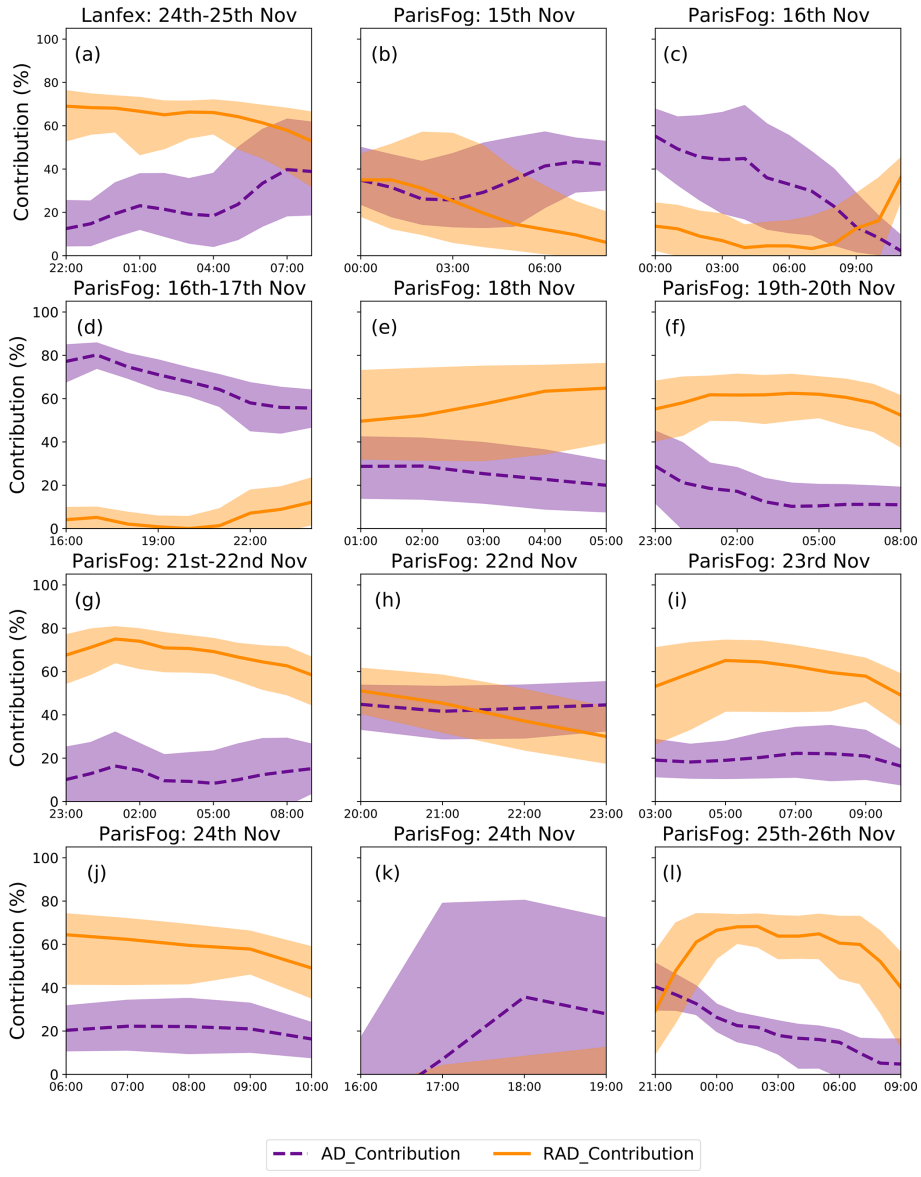

Figure 14. Time series (UTC) of the percentage contribution to droplet activation (at the surface) from radiative and adiabatic cooling, as simulated by our 500 m model across various fog cases during LANFEX **(a)** and ParisFog **(b–l)** campaigns. The dashed purple line represents the median fraction of droplets originating from adiabatic cooling while the solid orange line represents those originating from radiative cooling. Shaded regions illustrate the interquartile ranges of these contributions. The AD-RAD simulation is compared with the simulations AD and RAD to generate this figure.

nested simulations with the UK Met Office Unified Model. Our approach focuses on the contribution of radiative cooling to aerosol activation. Additionally, we conduct sensitivity studies to assess the impact of other possible effects on droplet number concentrations in our cases, such as that of droplet interception or of potential biases in our simulation of boundary layer turbulence and microphysics. We evaluated our model using time series of surface observations and balloon measurements of fog vertical structure. Our key findings are:

– *Our model simulates sufficient fog*: the 500 m model effectively simulates a considerable amount of fog across the domain for both the ParisFog and LANFEX cases. N_d and LWC are simulated to be lower in LANFEX compared to ParisFog, which broadly agrees with our observations, and our simulated LWP in LANFEX is in excellent agreement with the observations for simulations with activation via radiative cooling included. In common with other models, our model frequently did not correctly represent the time of fog onset or dissipa-

tion, and it also had little skill in representing temporal trends in surface LWC during individual fog events.

- *Radiative cooling is important for aerosol activation in fog*: we included a source of supersaturation from radiative cooling (together with a sink of supersaturation due to short-wave heating) into the activation scheme. With these changes, the simulated N_d overestimated the observations most of the time. On the assumption that the overestimate was equally attributable to radiative and adiabatic cooling, we calculated the relative importance of radiative and adiabatic cooling in fog and found that radiative cooling is often the dominant source, but both processes are frequently important for aerosol activation, depending on the conditions. The radiative cooling rates are variable in space and time and so cannot be properly represented by a fixed minimum updraft speed. Radiative cooling rates are always calculated by the radiation scheme in the model, independent of the activation process. Hence, including activation by radiative cooling should not significantly increase the computational cost. Similar to Poku et al. (2021), Peterka et al. (2024), and (less directly) Vié et al. (2024), our simulations highlight the possible importance of radiative cooling in the accurate representation of the droplet budget in the model.

- *Interception by trees and buildings is probably an important droplet sink*: in our first sensitivity study, we increased the sedimentation rate at the bottom most model level by a factor of 3 as a proxy for droplet interception. This process was not included in the model before and would need to be generalized to different surface types (for example, ocean) before it could be applied by default. When added to our model simulations with radiative cooling included, the change reduces bias in N_d and LWC. The high sensitivity of droplet concentrations to sedimentation rates corroborates the importance of fog deposition in the accurate prediction of the droplet life cycle, as explained by Mazoyer et al. (2022).

- *Suppression of activation via updrafts in inversions could also improve model performance*: in a second sensitivity study, we turned off activation by updrafts in temperature inversions, under the assumption that these updrafts are overestimated and therefore lead to excessive activation, similar to the findings of Boutle et al. (2018). We found that this change improved the model performance in most cases. If this modification were included in the model by default, together with radiative cooling in activation, the importance of radiative cooling in activation would likely be higher than the results we show in Sect. 4.6 suggest.

- *Overestimates in droplet concentrations could be mitigated if the concentrations slowly adjust to changes in supersaturation over time*: in our model simulations with radiative cooling included, we find that allowing droplets to deactivate in response to reductions in supersaturation over a relatively long but adjustable timescale leads to lower concentrations that agree better with observations. We term the timescale as the droplet concentration adjustment timescale (DCAT). We tested a 10 min timescale. The introduction of DCAT could serve as a proxy for missing processes in the model, such as droplet collision-coalescence or Ostwald ripening (Degefie et al., 2014; Mazoyer et al., 2019, 2022). While our model does not simulate the hygroscopic growth of haze aerosols accurately, as we discuss in the companion paper, if small droplets in our simulations can be considered a proxy for haze aerosols (which could also be detected as droplets by a fog monitor), then DCAT could also represent the possibility of these droplets shrinking in response to changes in relative humidity over time.

- *Simulation of fog top height is satisfactory in LANFEX and vertical structure could be realistic for an area average*: in our 500 m resolution simulations, the fog top height is simulated accurately in the model for the LANFEX case. In ParisFog, model performance may well be worse, but the comparison may be unfair as we compare measurements at a single point to an aggregate over a model domain. Simulations without radiative cooling generally simulate N_d well but the LWP is underestimated during LANFEX IOP1. With radiative cooling, agreement with observations is generally worse in simulating the vertical structure of N_d, but in good agreement for LWC. The sensitivity studies proves the model performance. The detailed vertical structure of LWC and N_d in the balloon measurements is not replicated by the model, but this is expected since these measurements are likely affected by highly localized fluctuations that are not simulated in detail by any model in the intercomparison study of Boutle et al. (2022) or in subsequent studies (e.g Vié et al., 2024).

Our two part publication aimed to explore strategies to realistically simulate fog droplet concentrations in a weather and climate model with prognostic aerosol microphysics. The companion paper focused on activation by adiabatic cooling during ParisFog while this paper focused on the role of radiative cooling in both ParisFog and LANFEX. We aimed to test only small modifications to the aerosol activation scheme rather than larger changes to the model structure that would be more likely to impact the computational cost of the model or its ability to simulate low clouds. Our tests yield a better understanding of the importance of different cooling sources for fog droplet activation in non-idealized cases. However, more fog events in different environments would need to be simulated before we can confidently recommend specific developments for new model releases. The contin-

uing high priorities are to simulate fog in pristine marine conditions, coastal fog, and ice fog. Furthermore, simulated updraft speeds for aerosol activation depend on horizontal grid resolution. In the simulations we present here, these updrafts are likely underestimated because we do not include a contribution from sub-grid-scale turbulence. While a scale-invariant parameterization of subgrid updraft velocity for the UM has been proposed (Malavelle et al., 2014), it still needs (at least) further testing and modification before it can be routinely used (Gordon et al., 2020). Thus, understanding how our parameterizations depend on domain resolution is an important task for the future. Finally, we also need to investigate how any changes to the activation scheme we recommend affect droplet concentrations in different cloud types. However, this work lays the foundations for improvements in aerosol activation in weather and climate models, with clear implications for the simulated optical properties and life cycle of fog.

Code and data availability. All model and observation data used in this work are available at: https://doi.org/10.5281/zenodo.15666154 (Ghosh et al., 2025b). All atmospheric simulations used in this work were performed using version 13.0 of the Met Office Unified Model (UM) starting from the GA7.1 configuration (Walters et al., 2019) alongside version 7.0 of JULES. The source code used in this study is free to use. However, software for this research is not publicly available due to intellectual property copyright restrictions, but is available to signatories of the Met Office Software license. Full descriptions of the software, including the specific configurations used in this study, can be found in the text of this article and in articles cited therein. A number of research organizations and national meteorological services use the UM in collaboration with the Met Office to undertake atmospheric process research, produce forecasts, develop the UM code, and build and evaluate Earth system models. To apply for a license for the UM, go to https://www.metoffice.gov.uk/research/approach/modelling-systems/unified-model (last access: 26 August 2025) and for permission to use JULES, go to https://jules.jchmr.org (last access: 26 August 2025). Rose and Cylc software were used to drive the Unified Model. The simulations were run using Rose version 2019.01.3 and Cylc version 7.8.8, which are publicly available at https://doi.org/10.5281/zenodo.3800775 (Shin et al., 2020), and https://doi.org/10.5281/zenodo.4638360 (Oliver et al., 2021) respectively. Both Rose and Cylc are available under v3 of the GNU General Public License (GPL). The full list of simulation identifiers for the simulations in this paper is given below.

- ParisFog Simulation Def-ARG:u-do390
- ParisFog Simulation AD: u-do373
- ParisFog Simulation AD-RAD: u-do549
- ParisFog Simulation AD-RAD-SED: u-do550
- ParisFog Simulation AD-RAD-INV: u-do554
- ParisFog Simulation AD-RAD-DCAT: u-do555
- ParisFog Simulation RAD: u-do551
- LANFEX Simulation Def-ARG: u-do761
- LANFEX Simulation AD: u-do762
- LANFEX Simulation AD-RAD: u-do763
- LANFEX Simulation AD-RAD-SED: u-do854
- LANFEX Simulation AD-RAD-INV: u-do855
- LANFEX Simulation AD-RAD-DCAT: u-dp007
- LANFEX Simulation RAD: u-dp008

Supplement. The supplement related to this article is available online at https://doi.org/10.5194/acp-25-11157-2025-supplement.

Author contributions. PG and HG formulated the idea of the paper with important contributions from all co-authors. PG and HG designed the simulations and set up different model configurations. MM supplied the data from the ParisFog field campaign. IB supplied the data from the LANFEX field campaign. PG ran all the simulations. PG analyzed the simulation and observation data with contributions from HG and wrote the paper with comments and suggestions from all co-authors.

Competing interests. The contact author has declared that none of the authors has any competing interests.

Disclaimer. Publisher's note: Copernicus Publications remains neutral with regard to jurisdictional claims made in the text, published maps, institutional affiliations, or any other geographical representation in this paper. While Copernicus Publications makes every effort to include appropriate place names, the final responsibility lies with the authors.

Acknowledgements. We thank the scientists responsible for the ParisFog and the LANFEX field campaigns. Model simulations are material produced using Met Office software. The computational resources on Air Force Weather HPC11 are provided by the Oak Ridge Leadership Computing Facility (OLCF) Director's Discretion Project NWP501 and ATM112. The OLCF at Oak Ridge National Laboratory (ORNL) is supported by the Office of Science of the US Department of Energy under contract no. DE-AC05-00OR22725. This work also used the Extreme Science and Engineering Discovery Environment (XSEDE), which is supported by the National Science Foundation Grant ACI-1548562. Specifically, it used the Bridges-2 system, which is supported by the NSF Award ACI-1928147, at the Pittsburgh Supercomputing Center (PSC). This work also used Bridges-2 at the PSC through allocation atm200005p from the Advanced Cyberinfrastructure Coordination Ecosystem: Services & Support (ACCESS) program, which is supported by National Science Foundation grants #2138259, #2138286, #2138307, #2137603, and #2138296.

Financial support. This research was supported by the US Air Force Life Cycle Management Center (LCMC) collaboration with Oak Ridge National Laboratory (ORNL).

Review statement. This paper was edited by Pablo Saide and reviewed by three anonymous referees.

References

Abdel-Aty, M., Ekram, A., Huang, H., and Choi, K.: A Study on Crashes Related to Visibility Obstruction Due to Fog and Smoke, Accident Anal. Prevent., 43, 1730–1737, https://doi.org/10.1016/j.aap.2011.04.003, 2011.

Abdul-Razzak, H. and Ghan, S.: A parameterization of aerosol activation: 2. Multiple aerosol types, J. Geophys. Res., 105, 6837–6844, https://doi.org/10.1029/1999JD901161, 2000.

Ackerman, A. S., Kirkpatrick, M. P., Stevens, D., and Toon, O. B.: The impact of humidity above stratiform clouds on indirect aerosol climate forcing, Nature, 432, 1014–1017, 2004.

Albrecht, B. A.: Aerosols, Cloud Microphysics, and Fractional Cloudiness, Science, 245, 1227–1230, https://doi.org/10.1126/science.245.4923.1227, 1989.

Archibald, A. T., O'Connor, F. M., Abraham, N. L., Archer-Nicholls, S., Chipperfield, M. P., Dalvi, M., Folberth, G. A., Dennison, F., Dhomse, S. S., Griffiths, P. T., Hardacre, C., Hewitt, A. J., Hill, R. S., Johnson, C E., Keeble, J., Köhler, M. O., Morgenstern, O., Mulcahy, J.P., Ordóñez, C., Pope, R. J., Rumbold, S. T., Russo, M. R., Savage, N. H., Sellar, A., Stringer, M., Turnock, S. T., Wild, O., and Zeng, G.: Description and evaluation of the UKCA stratosphere–troposphere chemistry scheme (StratTrop vn 1.0) implemented in UKESM1, Geosci. Model Dev., 13, 1223–1266, https://doi.org/10.5194/gmd-13-1223-2020, 2020.

Barahona, D. and Nenes, A.: Parameterization of cloud droplet formation in large-scale models: Including effects of entrainment, J. Geophys. Res.-Atmos., 112, https://doi.org/10.1029/2007JD008473, 2007.

Bergot, T., Terradellas, E., Cuxart, J., Mira, A., Liechti, O., Mueller, M., and Nielsen, N. W.: Intercomparison of Single-Column Numerical Models for the Prediction of Radiation Fog, J. Appl. Meteorol. Clim., 46, 504–521, https://doi.org/10.1175/JAM2475.1, 2007.

Boutle, I., Price, J., Kudzotsa, I., Kokkola, H., and Romakkaniemi, S.: Aerosol–fog interaction and the transition to well-mixed radiation fog, Atmos. Chem. Phys., 18, 7827–7840, https://doi.org/10.5194/acp-18-7827-2018, 2018.

Boutle, I., Angevine, W., Bao, J.-W., Bergot, T., Bhattacharya, R., Bott, A., Ducongé, L., Forbes, R., Goecke, T., Grell, E., Hill, A., Igel, A. L., Kudzotsa, I., Lac, C., Maronga, B., Romakkaniemi, S., Schmidli, J., Schwenkel, J., Steeneveld, G.-J., and Vié, B.: Demistify: a large-eddy simulation (LES) and single-column model (SCM) intercomparison of radiation fog, Atmos. Chem. Phys., 22, 319–333, https://doi.org/10.5194/acp-22-319-2022, 2022.

Bretherton, C. S., Blossey, P. N., and Uchida, J.: Cloud droplet sedimentation, entrainment efficiency, and subtropical stratocumulus albedo, Geophys. Res. Lett., 34, https://doi.org/10.1029/2006GL027648, 2007.

Brown, N., Weiland, M., Hill, A., Shipway, B., Maynard, C., Allen, T., and Rezny, M.: A Highly Scalable Met Office NERC Cloud Model, in: Proceedings of the 3rd International Conference on Exascale Applications and Software, University of Edinburgh, Edinburgh, UK, 132–137, https://dl.acm.org/citation.cfm?id=2820083.2820108 (last access: 5 May 2021), 2015.

Brown, N., Weiland, M., Hill, A., and Shipway, B.: In Situ Data Analytics for Highly Scalable Cloud Modelling on Cray Machines, Concurr. Comput.: Pract. Exp., 30, e4331, https://doi.org/10.1002/cpe.4331, 2018.

Bush, M., Flack, D. L. A., Lewis, H. W., Bohnenstengel, S. I., Short, C. J., Franklin, C., Lock, A. P., Best, M., Field, P., McCabe, A., Van Weverberg, K., Berthou, S., Boutle, I., Brooke, J. K., Cole, S., Cooper, S., Dow, G., Edwards, J., Finnenkoetter, A., Furtado, K., Halladay, K., Hanley, K., Hendry, M. A., Hill, A., Jayakumar, A., Jones, R. W., Lean, H., Lee, J. C. K., Malcolm, A., Mittermaier, M., Mohandas, S., Moore, S., Morcrette, C., North, R., Porson, A., Rennie, S., Roberts, N., Roux, B., Sanchez, C., Su, C.-H., Tucker, S., Vosper, S., Walters, D., Warner, J., Webster, S., Weeks, M., Wilkinson, J., Whitall, M., Williams, K. D., and Zhang, H.: The third Met Office Unified Model–JULES Regional Atmosphere and Land Configuration, RAL3, Geosci. Model Dev., 18, 3819–3855, https://doi.org/10.5194/gmd-18-3819-2025, 2025.

Clark, P. A., Harcourt, S. A., Macpherson, B., Mathison, C. T., Cusack, S., and Naylor, M.: Prediction of visibility and aerosol within the operational Met Office Unified Model. I: Model formulation and variational assimilation, Q. J. Roy. Meteorol. Soc., 134, 1801–1816, https://doi.org/10.1002/qj.318, 2008.

Danabasoglu, G., Lamarque, J.-F., Bacmeister, J., Bailey, D., Duvivier, A., Edwards, J., Emmons, L., Fasullo, J., Garcia, R., Gettelman, A., Hannay, C., Holland, M., Large, W., Lauritzen, P., Lawrence, D., Lenaerts, J., Lindsay, K., Lipscomb, W., Mills, M., and Strand, W.: The Community Earth System Model version 2 (CESM2), J. Adv. Model. Earth Syst., 12, https://doi.org/10.1029/2019MS001916, 2020.

Degefie, D. T., El-Madany, T., Hejkal, J., Held, M., Dupont, J.-C., Haeffelin, M., and Klemm, O.: Microphysics and energy and water fluxes of various fog types at SIRTA, France, Atmos. Res., 151, https://doi.org/10.1016/j.atmosres.2014.03.016, 2014.

Duconge, L., Lac, C., Vié, B., Bergot, T., and Price, J.: Fog in heterogeneous environments: the relative importance of local and non-local processes on radiative-advective fog formation, Q. J. Roy. Meteorol. Soc., 146, https://doi.org/10.1002/qj.3783, 2020.

Fast, J. D., Gustafson Jr., W. I., Easter, R. C., Zaveri, R. A., Barnard, J. C., Chapman, E. G., Grell, G. A., and Peckham, S. E.: Evolution of ozone, particulates, and aerosol direct radiative forcing in the vicinity of Houston using a fully coupled meteorology-chemistry-aerosol model, J. Geophys. Res.-Atmospheres, 111, https://doi.org/10.1029/2005JD006721, 2006.

Field, P. R., Hill, A., Shipway, B., Furtado, K., Wilkinson, J., Miltenberger, A., Gordon, H., Grosvenor, D. P., Stevens, R., and Van Weverberg, K.: Implementation of a Double Moment Cloud Microphysics Scheme in the UK Met Office Regional Numerical Weather Prediction Model, Q. J. Roy. Meteorol. Soc., 149, 703–739, 2023.

Ghosh, P., Evans, K. J., Grosvenor, D. P., Kang, H.-G., Mahajan, S., Xu, M., Zhang, W., and Gordon, H.: Assessing modifications to the Abdul-Razzak and Ghan aerosol activa-

tion parameterization (version ARG2000) to improve simulated aerosol–cloud radiative effects in the UK Met Office Unified Model (UM version 13.0), Geosci. Model Dev., 18, 4899–4913, https://doi.org/10.5194/gmd-18-4899-2025, 2025a.

Ghosh, P., Boutle, I., Field, P., Hill, A., Mazoyer, M., Evans, K., Mahajan, S., Kang, H.-G., Xu, M., Zhang, W., and Gordon, H.: Adiabatic and radiative cooling are both important causes of aerosol activation in simulated fog events in Europe, Zenodo [data set], https://doi.org/10.5281/zenodo.15666154, 2025b.

Ghosh, P., Boutle, I., Field, P., Hill, A., Jones, A., Mazoyer, M., Evans, K. J., Mahajan, S., Kang, H.-G., Xu, M., Zhang, W., Asch, N., and Gordon, H.: High sensitivity of simulated fog properties to parameterized aerosol activation in case studies from ParisFog, Atmos. Chem. Phys., 25, 11129–11156, https://doi.org/10.5194/acp-25-11129-2025, 2025c.

Golaz, J., Van Roekel, L., Zheng, X., Roberts, A., Wolfe, J., Lin, W., Bradley, A., Tang, Q., Maltrud, M., Forsyth, R., Zhang, C., Zhou, T., Zhang, K., Zender, C., Wu, M., Wang, H., Turner, A., Singh, B., Richter, J., and Bader, D.: The DOE E3SM Model Version 2: Overview of the Physical Model and Initial Model Evaluation, J. Adv. Model. Earth Syst., 14, https://doi.org/10.1029/2022MS003156, 2022.

Gordon, H., Field, P. R., Abel, S. J., Barrett, P., Bower, K., Crawford, I., Cui, Z., Grosvenor, D. P., Hill, A. A., Taylor, J., Wilkinson, J., Wu, H., and Carslaw, K. S.: Development of aerosol activation in the double-moment Unified Model and evaluation with CLARIFY measurements, Atmos. Chem. Phys., 20, 10997–11024, https://doi.org/10.5194/acp-20-10997-2020, 2020.

Gordon, H., Carslaw, K. S., Hill, A. A., Field, P. R., Abraham, N. L., Beyersdorf, A., Corr-Limoges, C., Ghosh, P., Hemmings, J., Jones, A. C., Sánchez, C., Wang, X., & Wilkinson, J.: NUMAC: Description of the Nested Unified Model With Aerosols and Chemistry, and Evaluation With KORUS-AQ Data, J. Adv. Model. Earth Syst., 15, e2022MS003457, https://doi.org/10.1029/2022MS003457, 2023.

Grell, G. A., Peckham, S. E., Schmitz, R., McKeen, S. A., Frost, G., Skamarock, W. C., and Eder, B.: Fully coupled "online" chemistry within the WRF model, Atmos. Environ., 39, 6957–6975, https://doi.org/10.1016/j.atmosenv.2005.04.027, 2005.

Grosvenor, D. P., Field, P. R., Hill, A. A., and Shipway, B. J.: The relative importance of macrophysical and cloud albedo changes for aerosol-induced radiative effects in closed-cell stratocumulus: insight from the modelling of a case study, Atmos. Chem. Phys. 17, 5155–5183, https://doi.org/10.5194/acp-17-5155-2017, 2017.

Gultepe, I., Tardif, R., Michaelides, S., Cermak, J., Bott, A., Bendix, J., Müller, M. D., Pagowski, M., Hansen, B., Ellrod, G. P., Jacobs, W., Toth, G., and Cober, S.: Fog Research: A Review of Past Achievements and Future Perspectives, Pure Appl. Geophys., 164, 1121–1159, 2007.

Haeffelin, M., Bergot, T., Elias, T., Tardif, R., Carrer, D., Chazette, P., Colomb, M., Drobinski, P., Dupont, E., Dupont, J.-C., Gomes, L., Musson-Genon, L., Pietras, C., Plana-Fattori, A., Protat, A., Rangognio, J., Raut, J.-C., Rémy, S., Richard, D., Sciare, J., and Zhang, X.: Parisfog: Shedding new Light on Fog Physical Processes, B. Am. Meteorol. Soc., 91, 767–783, https://doi.org/10.1175/2009BAMS2671.1, 2010.

Hao, W., Moghimi, B., Yang, X., Kamga, C., Wang, Y., Xiao, L., and Liu, Z.: Effects of foggy conditions on driver injury levels in U.S. highway-rail grade crossing accidents, Case Stud. Transp. Policy, 5, 627–633, https://doi.org/10.1016/j.cstp.2017.08.008, 2017.

Jayakumar, A., Gordon, H., Francis, T., Hill, A. A., Mohandas, S., Sandeepan, B. S., Mitra, A. K., and Beig, G.: Delhi Model with Chemistry and aerosol framework (DM-Chem) for high-resolution fog forecasting, Q. J. Roy. Meteorol. Soc., 147, 3957–3978, https://doi.org/10.1002/qj.4163, 2021.

Jia, X., Quan, J., Zheng, Z., Liu, X., Liu, Q., He, H., and Liu, Y.: Impacts of Anthropogenic Aerosols on Fog in North China Plain, J. Geophys. Res.-Atmos., 124, https://doi.org/10.1029/2018JD029437, 2019.

Jones, A. C., Hill, A., Remy, S., Abraham, N. L., Dalvi, M., Hardacre, C., Hewitt, A. J., Johnson, B., Mulcahy, J. P., and Turnock, S. T.: Exploring the sensitivity of atmospheric nitrate concentrations to nitric acid uptake rate using the Met Office's Unified Model, Atmos. Chem. Phys., 21, 15901–15927, https://doi.org/10.5194/acp-21-15901-2021, 2021.

Katata, G.: Fogwater deposition modeling for terrestrial ecosystems: A review of developments and measurements, J. Geophys. Res.-Atmos., 119, 8137–8159, 2014.

Kulkarni, R., Jenamani, R., Pithani, P., Konwar, M., Nigam, N., and Ghude, S.: Loss to Aviation Economy Due to Winter Fog in New Delhi During the Winter of 2011–2016, Atmosphere, 10, 198, https://doi.org/10.3390/atmos10040198, 2019.

Kutty, S. G., Dimri, A. P., and Gultepe, I.: Physical Processes Affecting Radiation Fog Based on WRF Simulations and Validation, Pure Appl. Geophys., 178, 4265–4288, https://doi.org/10.1007/s00024-021-02811-1, 2021.

Lac, C., Chaboureau, J.-P., Masson, V., Pinty, J.-P., Tulet, P., Escobar, J., Leriche, M., Barthe, C., Aouizerats, B., Augros, C., Aumond, P., Auguste, F., Bechtold, P., Berthet, S., Bielli, S., Bosseur, F., Caumont, O., Cohard, J.-M., Colin, J., Couvreux, F., Cuxart, J., Delautier, G., Dauhut, T., Ducrocq, V., Filippi, J.-B., Gazen, D., Geoffroy, O., Gheusi, F., Honnert, R., Lafore, J. P., Lebeaupin Brossier, C., Libois, Q., Lunet, T., Mari, C., Maric, T., Mascart, P., Mogé, M., Molinié, G., Nuissier, O., Pantillon, F., Peyrillé, P., Pergaud, J., Perraud, E., Pianezze, J., Redelsperger, J.-L., Ricard, D., Richard, E., Riette, S., Rodier, Q., Schoetter, R., Seyfried, L., Stein, J., Suhre, K., Taufour, M., Thouron, O., Turner, S., Verrelle, A., Vié, B., Visentin, F., Vionnet, V., and Wautelet, P.: Overview of the Meso-NH model version 5.4 and its applications, Geosci. Model Dev., 11, 1929–1969, https://doi.org/10.5194/gmd-11-1929-2018, 2018.

Lakra, K. and Avishek, K.: A Review on Factors Influencing Fog Formation, Classification, Forecasting, Detection and Impacts, Rendiconti Lincei, Scienze Fisiche e Naturali, 33, 319–353, https://doi.org/10.1007/s12210-022-01060-1, 2022.

Leung, A., Gough, W., and Butler, K.: Changes in Fog, Ice Fog, and Low Visibility in the Hudson Bay Region: Impacts on Aviation, Atmosphere, 11, 186, https://doi.org/10.3390/atmos11020186, 2020.

Malavelle, F. F., Haywood, J. M., Field, P. R., Hill, A. A., Abel, S. J., Lock, A. P., Shipway, B. J., and McBeath, K.: A method to represent subgrid-scale updraft velocity in kilometer-scale models: Implication for aerosol activation, J. Geophys. Res.-Atmos., 119, 4149–4173, https://doi.org/10.1002/2013JD021218, 2014.

Mann, G. W., Carslaw, K. S., Spracklen, D. V., Ridley, D. A., Manktelow, P. T., Chipperfield, M. P., Pickering, S. J., and

Johnson, C. E.: Description and evaluation of GLOMAP-mode: a modal global aerosol microphysics model for the UKCA composition-climate model, Geosci. Model Dev., 3, 519–551, https://doi.org/10.5194/gmd-3-519-2010, 2010.

Mann, G. W., Carslaw, K. S., Ridley, D. A., Spracklen, D. V., Pringle, K. J., Merikanto, J., Korhonen, H., Schwarz, J. P., Lee, L. A., Manktelow, P. T., Woodhouse, M. T., Schmidt, A., Breider, T. J., Emmerson, K. M., Reddington, C. L., Chipperfield, M. P., and Pickering, S. J.: Intercomparison of modal and sectional aerosol microphysics representations within the same 3-D global chemical transport model, Atmos. Chem. Phys., 12, 4449–4476, https://doi.org/10.5194/acp-12-4449-2012, 2012.

Maronga, B., Gryschka, M., Heinze, R., Hoffmann, F., Kanani-Sühring, F., Keck, M., Ketelsen, K., Letzel, M. O., Sühring, M., and Raasch, S.: The Parallelized Large-Eddy Simulation Model (PALM) Version 4.0 for Atmospheric and Oceanic Flows: Model Formulation, Recent Developments, and Future Perspectives, Geosci. Model Dev., 8, 2515–2551, https://doi.org/10.5194/gmd-8-2515-2015, 2015.

Mazoyer, M., Lac, C., Thouron, O., Bergot, T., Masson, V., and Musson-Genon, L.: Large eddy simulation of radiation fog: impact of dynamics on the fog life cycle, Atmos. Chem. Phys., 17, 13017–13035, https://doi.org/10.5194/acp-17-13017-2017, 2017.

Mazoyer, M., Burnet, F., Denjean, C., Roberts, G. C., Haeffelin, M., Dupont, J.-C., and Elias, T.: Experimental study of the aerosol impact on fog microphysics, Atmos. Chem. Phys., 19, 4323–4344, https://doi.org/10.5194/acp-19-4323-2019, 2019.

Mazoyer, M., Burnet, F., and Denjean, C.: Experimental study on the evolution of droplet size distribution during the fog life cycle, Atmos. Chem. Phys., 22, 11305–11321, https://doi.org/10.5194/acp-22-11305-2022, 2022.

Mulcahy, J. P., Jones, C. G., Rumbold, S. T., Kuhlbrodt, T., Dittus, A. J., Blockley, E. W., Yool, A., Walton, J., Hardacre, C., Andrews, T., Bodas-Salcedo, A., Stringer, M., de Mora, L., Harris, P., Hill, R., Kelley, D., Robertson, E., and Tang, Y.: UKESM1.1: development and evaluation of an updated configuration of the UK Earth System Model, Geosci. Model Dev., 16, 1569–1600, https://doi.org/10.5194/gmd-16-1569-2023, 2023.

Nelli, N., Francis, D., Abida, R., Fonseca, R., Masson, O., and Bosc, E.: In-situ measurements of fog microphysics: Visibility parameterization and estimation of fog droplet sedimentation velocity, Atmos. Res., 309, 107570, https://doi.org/10.1016/j.atmosres.2024.107570, 2024.

Oliver, H. J., Shin, M., Sanders, O., Fitzpatrick, B., Clark, A., Kinoshita, B. P., Dutta, R., Pillinger, T., Bartholomew, S. L., Hall, M., Valters, D., Sutherland, D., Trzeciak, T., challurip, Gaist, S., Matthews, D., Wales, S., ColemanTom, Menezes, G., Haiducek, J., Williams, J., lhuggett, Osprey, A., at BoM, J., Hatcher, R., Veselov, D., Reinecke, A., Andrew, Pulo, K., and Dix, M.: cylc/cylc-flow: cylc-7.8.8, Zendodo [code], https://doi.org/10.5281/zenodo.4638360, 2021.

Parde, A. N., Ghude, S. D., Sharma, A., Dhangar, N. G., Govardhan, G., Wagh, S., Jenamani, R., Pithani, P., Chen, F., Rajeevan, M., and Niyogi, D.: Improving simulation of the fog life cycle with high-resolution land data assimilation: A case study from WiFEX, Atmos. Res., 278, 106331, https://doi.org/10.1016/j.atmosres.2022.106331, 2022.

Peng, Y., Abdel-Aty, M., Lee, J., and Zou, Y.: Analysis of the Impact of Fog-Related Reduced Visibility on Traffic Parameters, J. Transp. Eng. Pt. A, 144, 04017077, https://doi.org/10.1061/JTEPBS.0000094, 2018.

Peterka, A., Thompson, G., and Geresdi, I.: Numerical prediction of fog: A novel parameterization for droplet formation, Q. J. Roy. Meteorol. Soc., 150, 2203–2222, https://doi.org/10.1002/qj.4704, 2024.

Pithani, P., Ghude, S., Prabha, T., Karipot, A., Hazra, A., Kulkarni, R., Chowdhuri, S., E A, R., Konwar, M., Murugavel, P., Safai, P., Chate, D., Tiwari, Y., Jenamani, R., and Rajeevan, M.: WRF model sensitivity to choice of PBL and microphysics parameterization for an advection fog event at Barkachha, rural site in the Indo-Gangetic basin, India, Theor. Appl. Climatol., 136, https://doi.org/10.1007/s00704-018-2530-5, 2019.

Poku, C., Ross, A., Blyth, A., Hill, A., and Price, J.: How important are aerosol-fog interactions for the successful modelling of nocturnal radiation fog?, Weather, 74, https://doi.org/10.1002/wea.3503, 2019.

Poku, C., Ross, A. N., Hill, A. A., Blyth, A. M., and Shipway, B.: Is a more physical representation of aerosol activation needed for simulations of fog?, Atmos. Chem. Phys., 21, 7271–7292, https://doi.org/10.5194/acp-21-7271-2021, 2021.

Prabhakaran, P., Shawon, A. S. M., Kinney, G., Thomas, S., Cantrell, W., and Shaw, R. A.: The role of turbulent fluctuations in aerosol activation and cloud formation, P. Natl. Acad. Sci. USA, 117, 16831–16838, https://doi.org/10.1073/pnas.2006426117, 2020.

Price, J.: On the Formation and Development of Radiation Fog: An Observational Study, Bound.-Lay. Meteorol., 172, 167–197, https://doi.org/10.1007/s10546-019-00444-5, 2019.

Price, J., Lane, S., Boutle, I., Smith, D., Bergot, T., Lac, C., Duconge, L., McGregor, J., Kerr-Munslow, A., Pickering, M., Clark, R.: LANFEX: a field and modeling study to improve our understanding and forecasting of radiation fog, B. Am. Meteorol. Soc., 99, 2061–2077, 2018.

Price, J. D., Vosper, S., Brown, A., Ross, A., Clark, P., Davies, F., Horlacher, V., Claxton, B., McGregor, J. R., Hoare, J. S., Jemmett-Smith, B., and Sheridan, P.: COLPEX: Field and Numerical Studies over a Region of Small Hills, B. Am. Meteorol. Soc., 92, 1636–1650, https://doi.org/10.1175/2011BAMS3032.1, 2011.

Seinfeld, J. H. and Pandis, S. N.: Atmospheric Chemistry and Physics, John Wiley, New York,, 1326 pp., ISBN 9781118947401, 1998.

Shin, M., Fitzpatrick, B., Clark, A., Sanders, O., Bartholomew, S. L., Whitehouse, S., Pillinger, T., Wardle, S., Matthews, D., Oxley, S., Trzeciak, T., Valters, D., Kinoshita, B. P., Mancell, J., harry shepherd, Oliver, H. J., Wales, S., Hall, M., Seddon, J., Osprey, A., Dix, M., Sharp, R., and Cresswell, P.: metomi/rose: 2019.01.3, Zenodo [code], https://doi.org/10.5281/zenodo.3800775, 2020.

Shipway, B. J. and Hill, A. A.: Diagnosis of systematic differences between multiple parametrizations of warm rain microphysics using a kinematic framework, Q. J. Roy. Meteorol. Soc., 138, 2196–2211, https://doi.org/10.1002/qj.1913, 2012.

Smith, R. N. B.: A scheme for predicting layer clouds and their water content in a general circulation model, Q. J. Roy. Meteor.

Soc., 116, 435–460, https://doi.org/10.1002/qj.49711649210, 1990.

Smith, D. K. E., Renfrew, I. A., Dorling, S. R., Price, J. D., and Boutle, I. A.: Sub-km Scale Numerical Weather Prediction Model Simulations of Radiation Fog, Q. J. Roy. Meteorol. Soc., 147, 746–763, https://doi.org/10.1002/qj.3943, 2021.

Smith, R. N. B.: A scheme for predicting layer clouds and their water content in a general circulation model, Q. J. Roy. Meteorol. Soc., 116, 435–460, https://doi.org/10.1002/qj.49711649210, 1990.

Stolaki, S., Haeffelin, M., Lac, C., Dupont, J.-C., Elias, T., and Masson, V.: Influence of aerosols on the life cycle of a radiation fog event. A numerical and observational study, Atmos. Res., 151, 146–161, https://doi.org/10.1016/j.atmosres.2014.04.013, 2015.

Stull, R. B.: An introduction to boundary layer meteorology, in: vol. 13, Springer Science & Business Media, https://doi.org/10.1007/978-94-009-3027-8, 1988.

Sullivan, S. C., Lee, D., Oreopoulos, L., and Nenes, A.: Role of updraft velocity in temporal variability of global cloud hydrometeor number, P. Natl. Acad. Sci. USA, 113, 5791–5796, https://doi.org/10.1073/pnas.1514039113, 2016.

Taylor, P. A., Chen, Z., Cheng, L., Afsharian, S., Weng, W., Isaac, G. A., Bullock, T. W., and Chen, Y.: Surface deposition of marine fog and its treatment in the Weather Research and Forecasting (WRF) model, Atmos. Chem. Phys., 21, 14687–14702, https://doi.org/10.5194/acp-21-14687-2021, 2021.

Twomey, S.: The Influence of Pollution on the Shortwave Albedo of Clouds, J. Atmos. Sci., 34, 1149–1152, https://doi.org/10.1175/1520-0469(1977)034<1149:TIOPOT>2.0.CO;2, 1977.

Vié, B., Ducongé, L., Lac, C., Bergot, T., and Price, J.: Importance of CCN activation for fog forecasting and its representation in the two-moment microphysical scheme LIMA, Q. J. Roy. Meteorol. Soc., https://doi.org/10.1002/qj.4812, 150, 4217–4234, 2024.

Walters, D., Baran, A. J., Boutle, I., Brooks, M., Earnshaw, P., Edwards, J., Furtado, K., Hill, P., Lock, A., Manners, J., Morcrette, C., Mulcahy, J., Sanchez, C., Smith, C., Stratton, R., Tennant, W., Tomassini, L., Van Weverberg, K., Vosper, S., Willett, M., Browse, J., Bushell, A., Carslaw, K., Dalvi, M., Essery, R., Gedney, N., Hardiman, S., Johnson, B., Johnson, C., Jones, A., Jones, C., Mann, G., Milton, S., Rumbold, H., Sellar, A., Ujiie, M., Whitall, M., Williams, K., and Zerroukat, M.: The Met Office Unified Model Global Atmosphere 7.0/7.1 and JULES Global Land 7.0 configurations, Geosci. Model Dev., 12, 1909–1963, https://doi.org/10.5194/gmd-12-1909-2019, 2019.

Xue, Y., Wang, L.-P., and Grabowski, W. W.: Growth of Cloud Droplets by Turbulent Collision–Coalescence, J. Atmos. Sci., 65, 331–356, https://doi.org/10.1175/2007JAS2406.1, 2008.

Yan, S., Zhu, B., Zhu, T., Shi, C., Liu, D., Kang, H., Lu, W., and Lu, C.: The Effect of Aerosols on Fog Lifetime: Observational Evidence and Model Simulations, Geophys. Res. Lett., 48, https://doi.org/10.1029/2020GL091156, 2021.

Yang, F., Kollias, P., Shaw, R. A., and Vogelmann, A. M.: Cloud droplet size distribution broadening during diffusional growth: ripening amplified by deactivation and reactivation, Atmos. Chem. Phys., 18, 7313–7328, https://doi.org/10.5194/acp-18-7313-2018, 2018.

Zhao, L., Niu, S., and Yu, F.: Microphysical characteristics of sea fog over the east coast of Leizhou Peninsula, China, Adv. Atmos. Sci., 30, https://doi.org/10.1007/s00376-012-1266-x, 2013.